INSPIRE-ETN
INSPIRING PRESSURE GAIN COMBUSTION INTEGRATION RESEARCH, AND EDUCATION

DELIVERABLE D 5.2 TEST OF TRANSEO CODE, EQUIPPED WITH LITERATURE PERFORMANCE MAPS

GRANT AGREEMENT NUMBER:	956803
PROJECT ACRONYM:	INSPIRE
PROJECT TITLE:	INSPIRING PRESSURE GAIN COMBUSTION INTEGRATION, RESEARCH AND EDUCATION
START DATE OF THE PROJECT:	1st January, 2021
DURATION OF THE PROJECT:	48 MONTHS
WORKPACKAGE:	WP5
LEAD BENEFICIARY:	UNIGE
DELIVERABLE LEADER:	UNIGE
DELIVERABLE AUTHORS	Sreenath Purushothaman, A. Sorce, A. Traverso
DISSEMINATION LEVEL:	PU - Public
DELIVERABLE TYPE:	Other
DUE DATE OF DELIVERABLE:	M20
ACTUAL SUBMISSION DATE:	M23
REFERENCE:	INSPIRE_ 11-2022_D5.2_Rev.0

Abstract:

Modelling of aircraft engines at system level is one of the most important steps in the development of engine architectures and control systems. Most of the software tools available today are capable of steady and transient simulations of engines but fall short when dynamic analysis is required, especially during unstable or unsteady operating regimes, such as those driven by PGC technology. TRANSEO simulation tool, developed by University of Genova, is a solution to this problem. Under the INSPIRE project activities at UNIGE, the TRANSEO code has been used to model a typical aircraft engine. The model has been validated with on-design & off-design engine performance test results. In addition, a multistage compressor model is also developed, which is capable of predicting compressor surge. The advantages and limitations of the code and modelling methodology have been identified, and measures are being taken to improve the model to simulate aircraft engines with PGC technology.

TABLE OF CONTENTS

LIST OF FIGURES

LIST OF TABLES

GLOSSARY

Acronym	Description
EGT	Exhaust Gas Temperature
HP	High Pressure
HPC	High Pressure Compressor
HPT	High Pressure Turbine
HPTCC	High Pressure Turbine Clearance Control
IGV	Inlet Guide Vane
LP	Low Pressure
LPC	Low Pressure Compressor
LPT	Low Pressure Turbine
MoC	Method of Characteristics
N1	Low Pressure spool speed
N2	High Pressure spool speed
OGV	Outlet Guide Vane
PDC	Pulse Detonation Combustion
PGC	Pressure Gain Combustion
RDC	Rotating Detonation Combustion
RPM	Revolutions per minute
SAE	Society of Automobile Engineers
UNIGE	Università degli Studi di Genova
VBV	Variable Guide Vane
VSV	Variable Stator Vane

Table 1 : List of acronyms

EXECUTIVE SUMMARY

The following report is a description of the research activities conducted under the topic "PGC propulsion application with part load and dynamic analysis" at University of Genova, Italy to develop the deliverable titled "Test of TRANSEO Code, equipped with literature performance maps". The research activities include the development of a multistage compressor dynamic model, capable of demonstrating the surge and stall phenomenon, and the development of a high bypass, turbofan engine model using TRANSEO simulation tool, basing on industrial partners guidance. The models have been validated against the data available on public domain and are found to be satisfactory towards the goal of simulating aircraft engines. The advantages and limitations of using TRANSEO to model complex engineering systems such as aircraft engines have been identified. This knowledge is deemed useful in the continuing endeavor to develop propulsion system dynamic models using PGC technologies.

INTRODUCTION

A large number of research work have been ongoing in the field of gas turbine engines in the recent decades to improve their efficiency and specific work and thus reduce fuel consumption and emissions [1–6]. A solution for the isobaric heat addition process in the Brayton cycle, where there is a pressure loss in the combustion process, is the implementation of Pressure Gain Combustion (PGC). The PCG technologies use gas dynamic waves to confine the combustion process and thereby achieve an approximately constant volume combustion, which has higher thermodynamic cycle efficiency than the conventional Brayton cycle[7–10].

The goal of this research work is to study the effects of gas dynamic phenomena in PGC at cycle level and to identify the operational limitations with regards to propulsion application. The effects of gas dynamic cross-interference and the resulting instabilities will be studied in order to develop an operational envelop for the PGC gas turbine. The research work would yield a full performance map at variable ambient conditions of a PGC simple cycle gas turbine, consisting of real processes, considering the unsteadiness and possible feedback loops in the gas turbine operation, optimized to get maximum thermodynamic efficiency and specific impulse, and minimum emission. The research would also result in the detailed description of the dynamic performance of the PGC cycle gas turbine and the development of control concepts for the engine.

DEVELOPMENT OF A MULTISTAGE COMPRESSOR DYNAMIC MODEL

3.1. Introduction

A 1-D reduced order model of a multistage, axial compressor is being developed to understand the gas dynamic instabilities and operational envelop when integrating with a PGC combustor such as RDE combustor. The model will be able to utilize the unsteady flow parameters at the combustor inlet and compressor bleed for engine cooling to provide information regarding the surge and stall instabilities that may be encountered during PGC propulsion engine operation.

The model can be used as a standalone compressor connected to a plenum chamber, or with upstream and downstream components of an aircraft engine. The model requires as inputs the compressor stage characteristics maps, geometry details, simulation parameters including Greitzer parameter, back-pressure variation details, and solves the numerical problem with a MacCormack Predictor-Corrector method for steady and transient cases. Relevant open literature papers are referenced in the next section.

3.2. Literature Review

The compression system performance is an important parameter for the gas turbines. The air delivery from a compressor is useful only if the compression system is in stable operation. The aerodynamic instabilities such as surge and/or rotating stall have been observed in the compressors. Surge is a violent planar disturbance in which the flow in the compressor reverses direction. Rotating stall occurs when a portion of the circumferential annulus is locally stalled by some destabilizing event such as a low-pressure region[11].

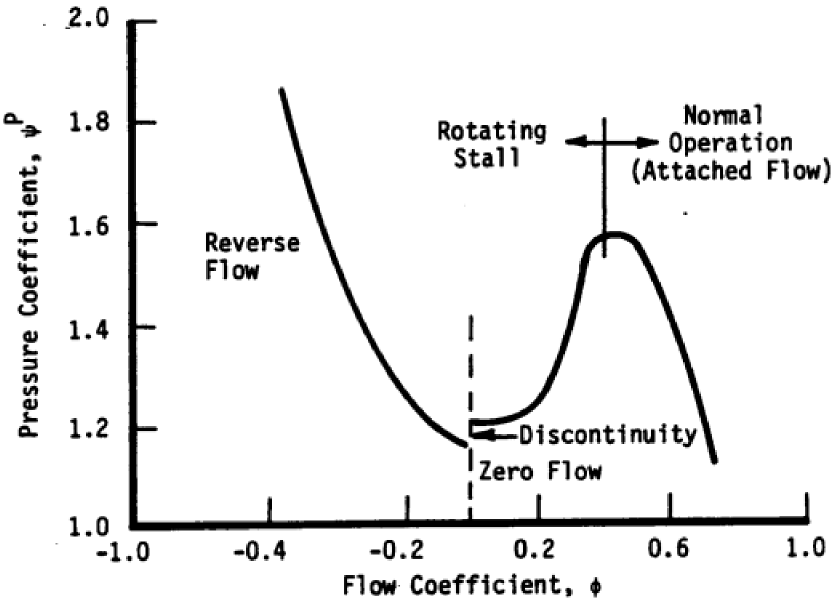

Figure 1 –Typical operating regions of a compressor [11]

Greitzer and Moore [12,13], Gamache [14], Haynes [15] and others have done significant research on understanding the surge mechanism. Greitzer has developed a non-dimensional parameter to characterize surge in compressors.

Although Greitzer's model using parallel compressor theory is a widely accepted model, it is unable to completely capture the phenomenon in a multistage compressor. This includes the effect of bleed and interstage gas dynamic instabilities. Davis [11], Massardo and Cravero[16,17], Soria [18] and others have approached this problem by utilizing 1-D Euler equations to model the compressor. The problem with this approach is that it requires detailed geometry and stage characteristics of the compression system.

In this work, a multistage axial compressor is modelled using a combination of 1-D and 0-D methods, where the geometry and operating conditions of the compression system are approximated from the available experimental data.

3.3. Modelling the compressor (standalone configuration)

The compressor is represented as a quasi-1-Dimensional model, where the variation of flow properties is assumed to be uniform across each section. A 0-Dimensional plenum is assumed to be present at the compressor exit with a throttle valve attached to it, allowing the flow rate to be controlled. This configuration is selected to verify the model with experimental data and is termed as standalone configuration in this report.

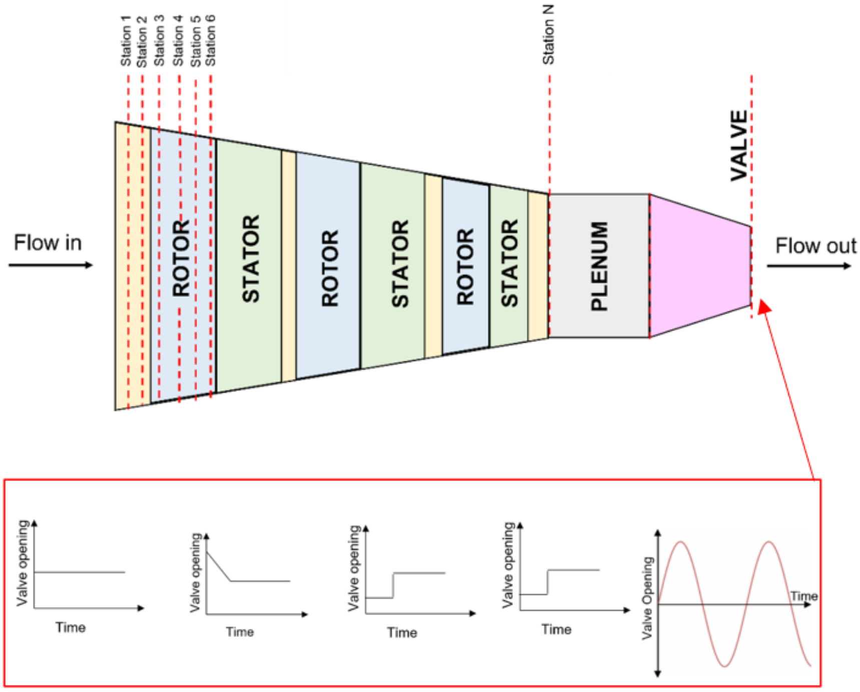

Figure 2 - Representation of multistage, axial compressor (standalone configuration)

When an engine uses PGC technologies, the compressor outlet may experience sudden and large amplitude pressure fluctuations, such as in the case of RDC or PDC. In order to ensure that the model can handle such fluctuations, the plenum throttle valve operation has the option to simulate different types of operational schedules, as shown in Figure 2. The model is also capable of simulating interstage air bleed.

The variation of the plenum throttle valve area causes backpressure fluctuations at the compressor exit. This causes the compressor to operate near stall speeds. Once the compressor mass flow rate falls below the stall condition, it undergoes stall and surge cycles, and depending on the operating parameters, may go into reverse flow condition. The model is able to predict this behavior, provided that the individual stage characteristics, flow path area, and other simulation parameters are available.

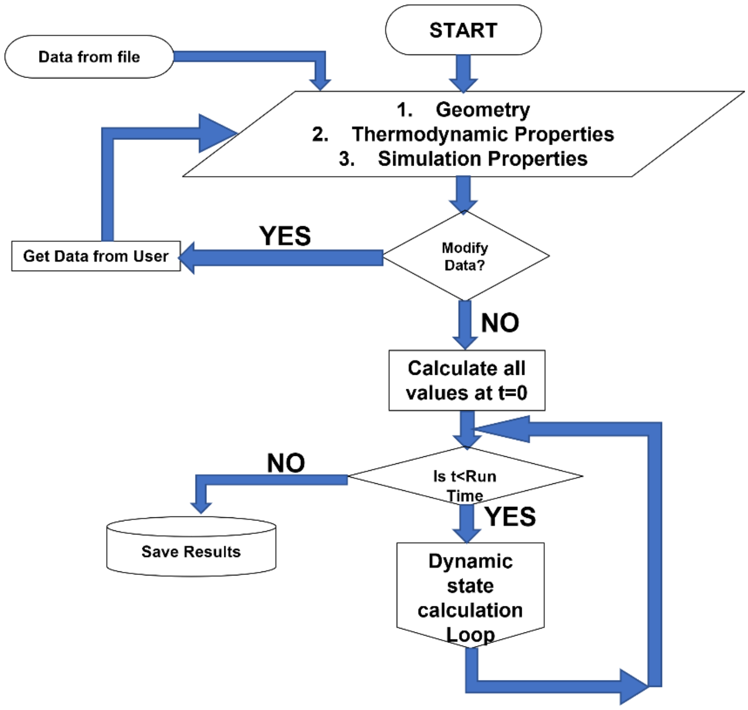

Figure 3 – Modelling flow chart

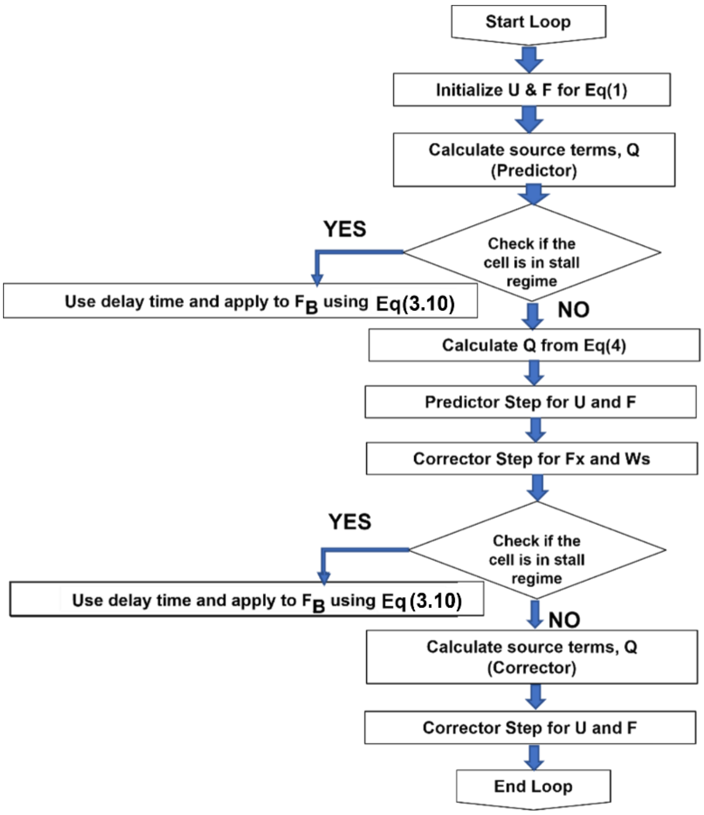

Figure 4 – Dynamic modelling strategy

The compressor model is developed using 1-D unsteady Euler equations, as represented in Figure 3 and Figure 4. The governing equations are as shown.

$$\frac{\partial \boldsymbol{U}}{\partial \boldsymbol{t}} + \frac{\partial \boldsymbol{F}}{\partial \boldsymbol{x}} = \boldsymbol{Q} \tag{3.1}$$

$$\mathbf{U} = \begin{bmatrix} \rho A \\ \rho u A \\ \rho A\left(e + \frac{u^2}{2}\right) \end{bmatrix} \tag{3.2}$$

$$\mathbf{F} = \begin{bmatrix} \rho u A \\ (P + \rho u^2)A \\ \rho A u\left(e + \frac{u^2}{2} + \frac{P}{\rho}\right) \end{bmatrix} \tag{3.3}$$

$$\mathbf{Q} = \begin{bmatrix} -\dot{m}_b \\ F_X \\ -H_b + W_S + \dot{Q} \end{bmatrix} \tag{3.4}$$

$$F_X = F_B + P_s \frac{\partial A}{\partial x} \tag{3.5}$$

$$F_B = (P_{se}A_e - P_{si}A_i) \tag{3.6}$$

$$P_{Se} = \left(\psi^P \times \frac{1}{2} \times \rho_{0a} \times {U_m}^2\right) + P_{Si} \tag{3.7}$$

$$W_s = \frac{{U_m}^2}{2C_p} \times \psi^T \tag{3.8}$$

$$P = \rho R T \tag{3.9}$$

$$F_{XS} = \tau \frac{\partial F_X}{\partial t} + F_X \tag{3.10}$$

$$\tau = \frac{2\pi R_m n}{U_m} \tag{3.11}$$

3.4. Treatment of Boundary Conditions for standalone compressor model

Since the predictor-corrector scheme requires the conditions at the boundaries to be known at each time step, the boundary conditions are calculated using Method of Characteristics for the standalone model. At compressor inlet, the stagnation pressure and stagnation temperature are the input terms while at the exit, the static pressure is the input term.

The compatibility equations are solved along the characteristics curve for the MoC (Figure 5) to obtain the boundary conditions. The outlet static pressure is calculated by a mass balance between compressor outlet flow and flow through the plenum exit throttle valve as shown in Eq (3.12). The plenum is modelled as 0-D to reduce the computational effort. In case of reverse flow, the inlet boundary switches to subsonic outlet with ambient static pressure as the fixed parameter.

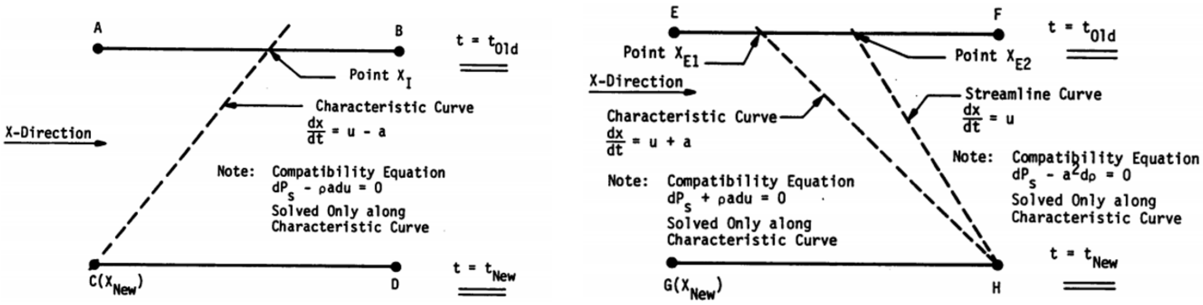

Figure 5 - MoC boundary treatment for a) Inlet b) Outlet [11]

$$\dot{m}_C - \dot{m}_T = \frac{\rho V_P}{\gamma P_P} \frac{dP_P}{dt} \qquad (3.12)$$

3.5. Compressor stage characteristics and steady-state operation

The model validation is done using the experimental results from Greitzer [13] and Gamache [14]. The compressor used for the surge experiments by Greitzer is a 3- stage compressor having repeating stage blading and constant area, fitted with a variable plenum, as shown in Figure 6 [13]. The details of the test rig are given in Table 2.

Hub diameter	0.6096 m
Hub-to-tip ratio (Greitzer's setup)	0.7
Blade airfoil	NACA 400 series
Nominal Speed	5926 rpm
Mean blade speed	177.8 m/s
Flow coefficient	0.619
Total Pressure Ratio	1.489
Efficiency	86.2 %

Table 2 : Details of Greitzer's compressor [11]

Unfortunately, some of the crucial details of this compression system, such as length of the compressor and intake duct, and throttle valve closing schedule were not available from the literature. The experimental stage characteristics curves developed by Gamache [11,14] (Figure 7) are used to simulate the compressor nominal operation, although it had a Hub-to-tip ratio of 0.88. The plenum exit valve is then closed to the point of surge instability, and the transient simulation is run. Since the stage temperature rise is not directly available from experiments, it needs to be synthesized from stage torque coefficient. The stage temperature characteristics synthesized by Davis [11] has been used for this purpose (Figure 8).

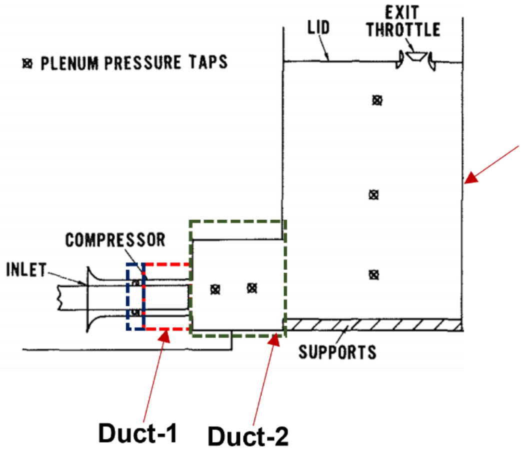

Figure 6 – Schematic of the compressor system used by [13]

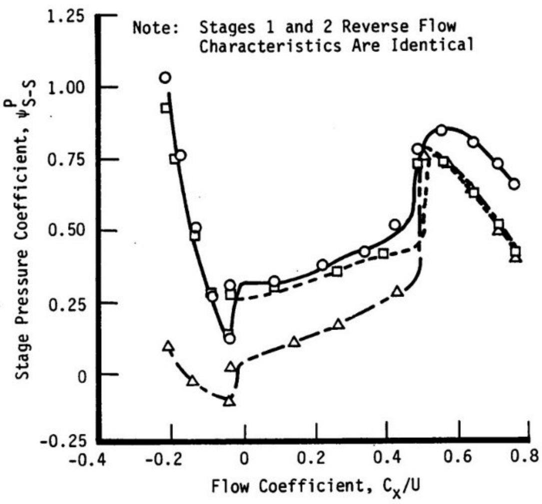

Figure 7 – Experimental stage pressure characteristics[11]

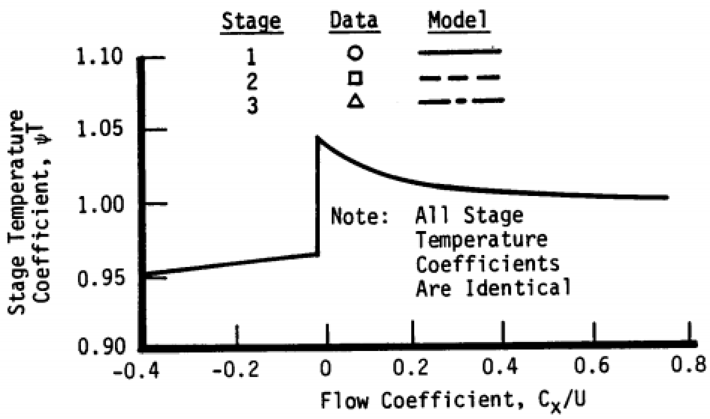

Figure 8 – Synthesized stage temperature characteristics [11]

The model is run with these characteristics to obtain a steady state operating point, defined using a design flow coefficient (Figure 9).

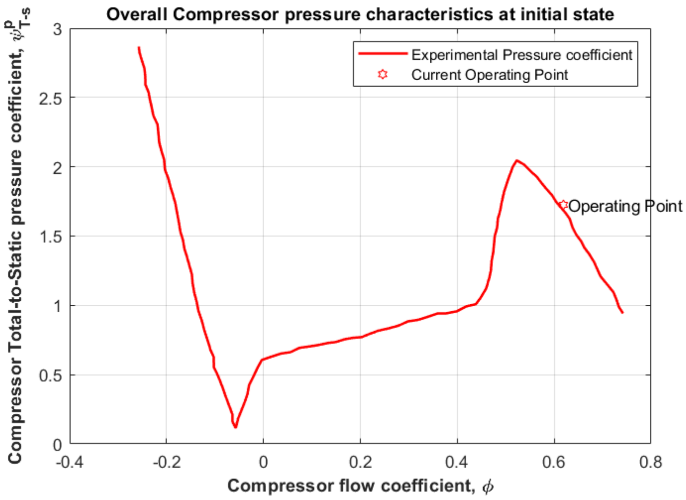

Figure 9 – Steady state operating condition for B=0.66

3.6. Transient Simulation and Results

Once the steady state operating point is obtained, the plenum throttle is closed to initiate surge. The response of the compressor to the throttle closure depends on various parameters such as plenum volume, compressor equivalent length, time delay, mean rotor velocity etc. Some of these parameters are grouped into the non-dimensional Greitzer's parameter, B. The effect of throttle closure, delay time and B are discussed below.

3.6.1. Effect of Greitzer's parameter, B

The non-dimensional parameter B, introduced by Greitzer, is used to classify the nature of the surge for a specific compressor. B is defined as:

$$\boldsymbol{B} = \frac{\boldsymbol{U_m}}{\boldsymbol{2a}}\sqrt{\frac{\boldsymbol{V_P}}{\boldsymbol{A_C L_c}}} \qquad (3.13)$$

where, U_m = mean blade speed , a = *speed of sound* , V_P = *plenum volume* , A_C = *compressor cross section area*, L_c = *equivalent length of compressor ducts.*

Sl. No	B	Lc	Vp	Delay time parameter(n)	Um	Throttle closing	Frequency
		m	m^3		m/s	% of design point A_T	Hz
1	0.660	0.762	6.840	2.000	59.020	60.000	NA
2	1.000	0.728	15.000	3.000	59.020	82.700	0.975
3	1.040	0.762	6.840	3.151	92.980	80.200	2.091

Table 3 : Simulation parameters for B parameter test

The model is set up for different values of B as shown in Table 3. The resulting plots and frequencies are compared against the data available from literature (Figure 11). The equivalent duct length L_C and speed of sound were not mentioned in the experimental data [11,13], thereby making the comparison difficult. A value of 300 K, and 101325 Pa (abs) are used as the operating temperature and total pressure of the ambient, and 100000 Pa (abs) as plenum exit pressure.

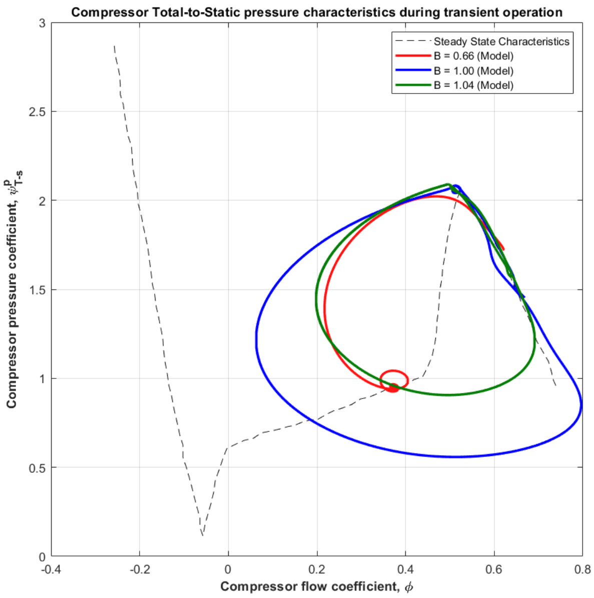

Figure 10 – Effect of B on surge response

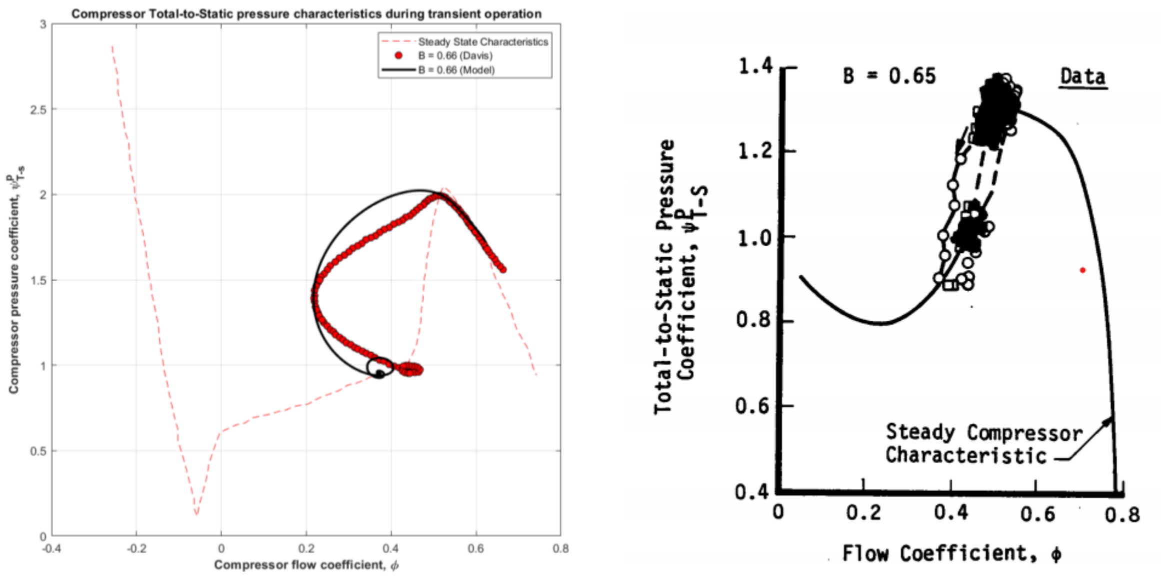

(a) (b)

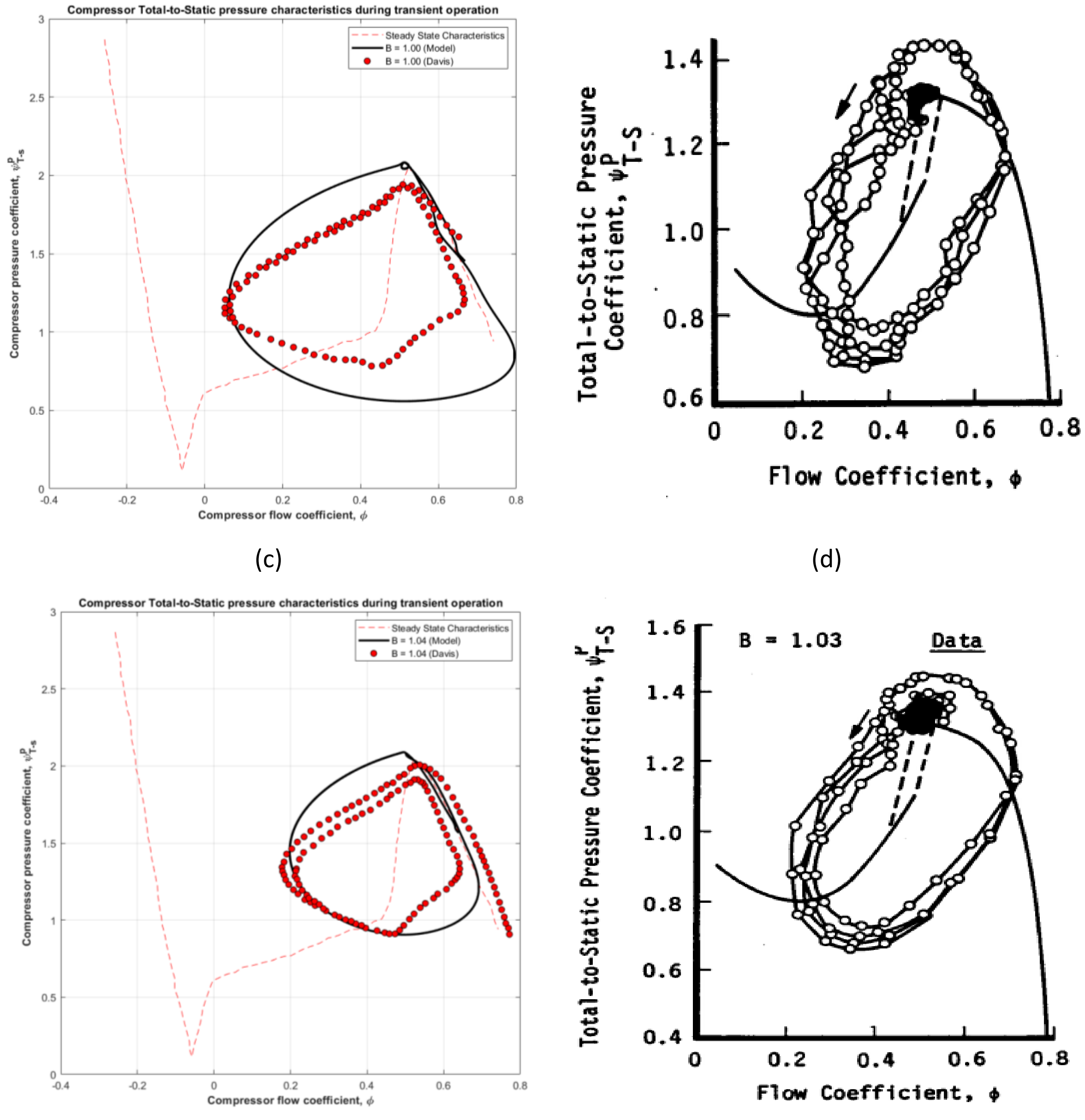

(e) (f)

Figure 11 – Surge response comparison

The surge responses of the compressor under different B parameters are shown in Figure 10. The comparison of these responses with experimental results from Gamache [14] and Davis [11] are discussed in detail below.

The comparison of the simulation results from current model and Davis [11], shown in Figure 11 (a), with experimental results from Greitzer [13] in Figure 11 (b), shows that for B ≈ 0.65 (Table 3), the compressor becomes unstable after the stall point when the throttle is closed to 60% of the on-design operating point with n=2 for time delay and settles down at a new operating point. The fluctuations of flow coefficient are also similar as shown in Figure 12 (a) from model and in Figure 12 (b) from experiments[13]. The delay time (τ) calculated from Eq 3.11 for n=2 is kept same for the rest of the simulations, as mentioned in Greitzer [13].

For B = 1.00, the compressor moves from its on-design point once the throttle is closed sufficiently (Table 3) and enters a surge cycle (Figure 11 (c)). This behaviour is very similar to that observed by Greitzer [13](Figure 11 (d)).The frequency of flow coefficient during surge is 0.975 Hz from the current model and Davis[11] (Figure 12 (c)) while it is approximately 1 Hz from the experiments Figure 12 (d) [13].

The compressor rig was configured to high speed, small plenum operation, and this obtained a B = 1.03 [11]. The model is also configured to simulate this condition (Table 3) as per the velocity & plenum volume used by Davis [11]. The surge response obtained by the model is similar to that by Davis [11] as shown in Figure 11 (e) and from experiments by Greitzer [13] as in Figure 11 (f). The corresponding flow coefficient fluctuation is shown in Figure 12 (e).

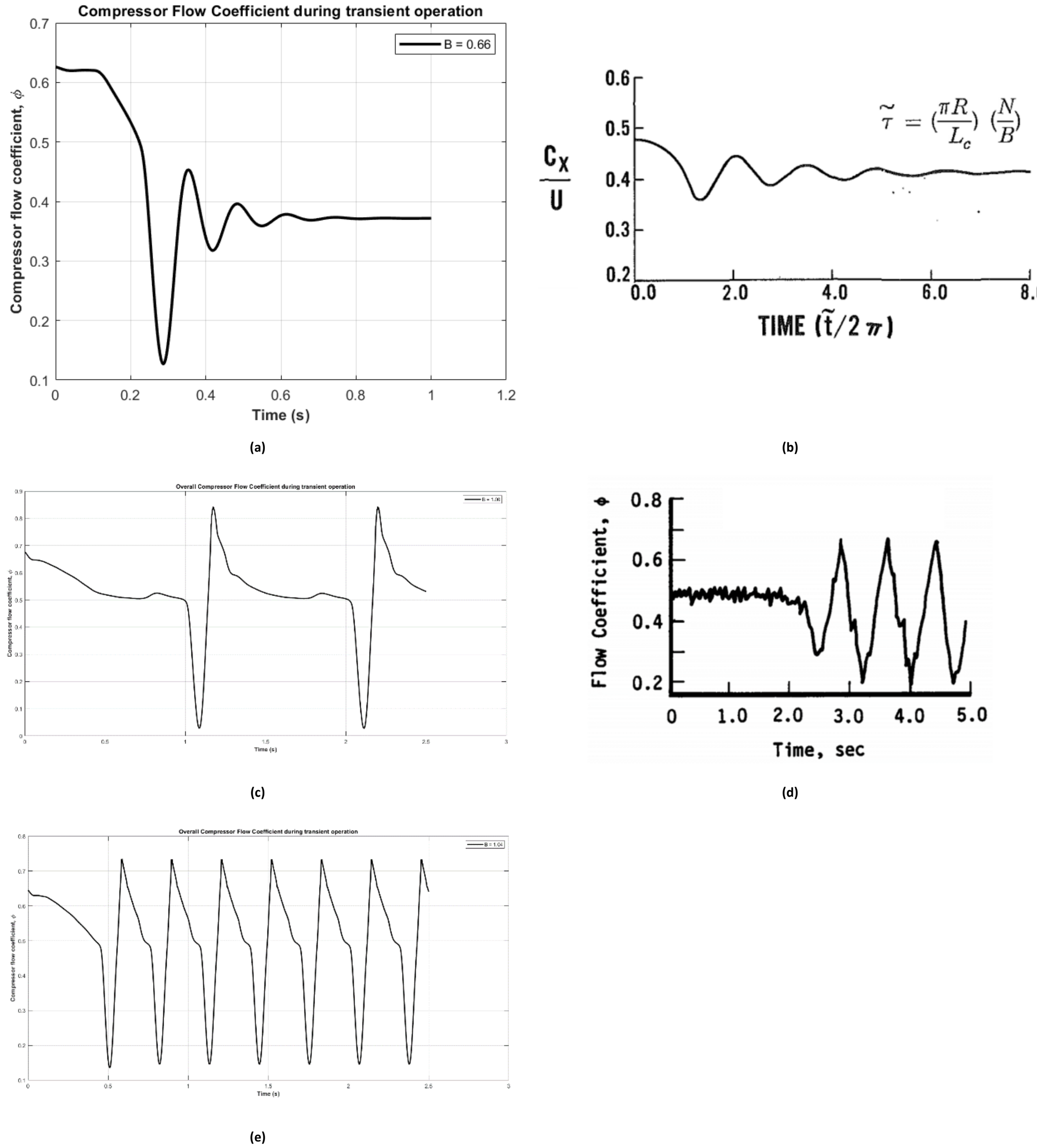

Figure 12 – Flow coefficient fluctuations for different B parameter

It is to be noticed that the plenum volumes used by Greitzer in his experiments as specified in [13] and the ones used in the model is different. This is because of the necessity for model similarity between the experiment and the model compressor characteristics. This variation arises due to the use of characteristics for different compressor blading by Greitzer and Gamache, as reported in [11] and [13].

3.6.2. Effect of throttle closure

Greitzer[13] and Davis [11] notice that the final position of the throttle valve can affect the nature of the surge and its frequency. In the current model, the effect of throttle closure point has been investigated. The exact throttle closure point and schedule was not available from literature, hence this parameter had to be approximated.

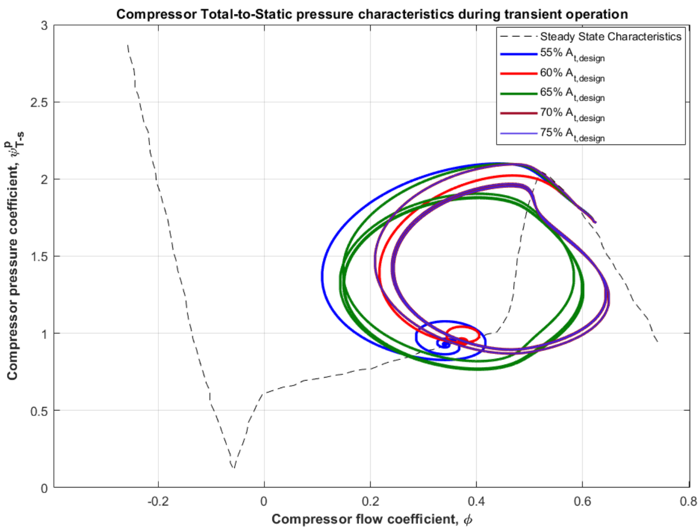

Figure 13 – Effect of final throttle position on surge response

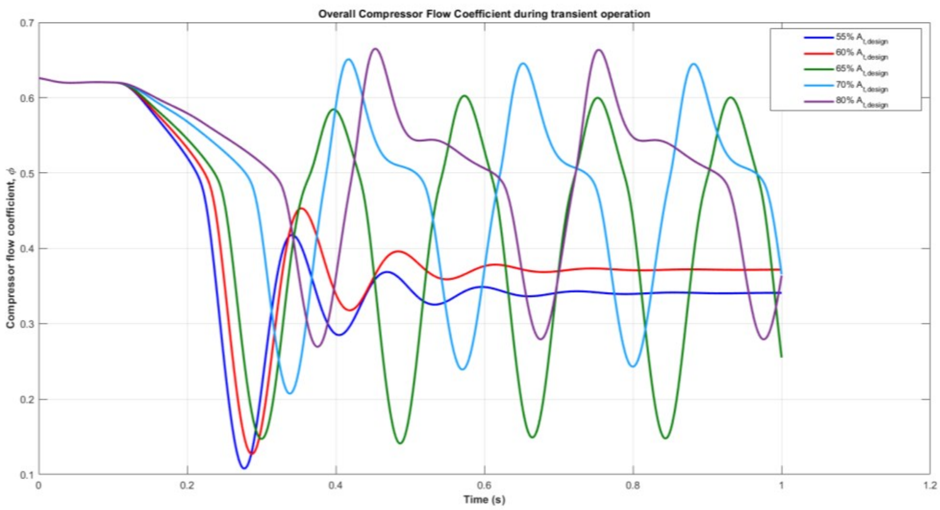

Figure 14 – Effect of final throttle position on surge cycles

Sl.No	B	Lc	Vp	Delay time parameter (n)	Um	Throttle closing point
		m	m^3		m/s	% of design point $A_{throttle}$
1	0.660	0.762	6.840	2.000	59.020	55.0
2	0.660	0.762	6.840	2.000	59.020	60.0
3	0.660	0.762	6.840	2.000	59.020	65.0
4	0.660	0.762	6.840	2.000	59.020	70.0
5	0.660	0.762	6.840	2.000	59.020	75.0

Table 4 : Effect of throttle closing point

The model is configured for B = 0.66, with a time delay corresponding to n= 2 (from Eq 3.11). The throttle is closed from the on-design point ($A_{throttle}$) up to 55% of on-design point. The surge response is shown in Figure 13 and Figure 14 . It is evident that the final position of the throttle has a significant effect on the amplitude and frequency of surge response. This creates a limitation on the validation of the model when the exact valve position is unknown.

3.6.3. Effect of delay time

In order to capture the dynamics of surge phenomenon, a first order delay time (τ) is introduced into the governing equations. This delay time represents the time it takes for the stall cells to form around the rotor annulus, and this is usually an experimental parameter. Greitzer[13] defined the delay time as a function of number of rotations (n in Eq 3.11) it takes for the stall cells to cover a significant portion of the annulus.

Sl.No	B	Lc	Vp	Delay time parameter (n)	Um	At_closepoint
		m	m^3		m/s	% of design point $A_{throttle}$
1	0.660	0.762	6.840	10.000	59.020	60.000
2	0.660	0.762	6.840	8.000	59.020	60.000
3	0.660	0.762	6.840	6.000	59.020	60.000
4	0.660	0.762	6.840	4.000	59.020	60.000
5	0.660	0.762	6.840	2.000	59.020	60.000

Table 5 : Effect of delay time

For the compressor used for validation, Greitzer reports a value of n equal to 2. But it is interesting to see the effect of this delay time on the surge response. The simulation is conducted by fixing B = 0.66 and the throttle is closed to 60% of the on-design steady state condition (Table 5). As shown in Figure 15, for values of n greater than 2 the compressor follows a different response pattern. Thus, it is clear that the choice of delay time should not be an arbitrary value, as this would affect the nature of the surge response.

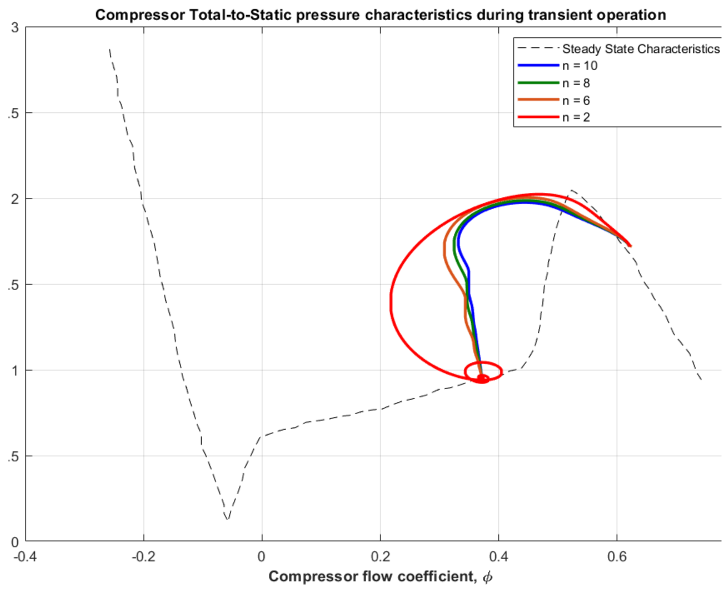

Figure 15 – Effect of delay time on compressor surge

3.6.4. Effect of equivalent duct length, Lc

The non-dimensional parameter B, introduced by Greitzer, is used to classify the nature of the surge for a specific compressor. B is defined as in Eq 3.13. It is to be noted that mathematically, the values of these variables can be changed while maintaining the same B. If B would be the only parameter driving the transient, it should be expected that different combinations of parameter bringing to the same B value would result in similar surge transients. Unfortunately, this is not the case, as demonstrated by the following results, where B is kept constant with different values of the equivalent duct length Lc and plenum volume Vp (Table 6).

Sl.No	B	Lc	Ac	Vp	Delay time parameter (n)	Um	At_closepoint
		m	m^2	m^3		m/s	% of design point $A_{throttle}$
1	0.660	0.200	0.149	1.795	2.000	59.020	60.000
2	0.660	0.300	0.149	2.693	2.000	59.020	60.000
3	0.660	0.400	0.149	3.591	2.000	59.020	60.000
4	0.660	0.600	0.149	5.386	2.000	59.020	60.000
5	0.660	0.762	0.149	6.840	2.000	59.020	60.000
6	0.660	0.800	0.149	7.181	2.000	59.020	60.000

Table 6 ; Effect of equivalent length & plenum volume

As demonstrated in Figure 16 , basing on the simulation results alone, B parameter is specific to a compressor model and experimental set-up, and, unfortunately, there is a knowledge gap in determining a separate influence on surge behavior by the geometrical parameters included in the B definition. This is reflected in the difficulty of comparing the experimental results, since the equivalent duct length L_C and speed of sound, a, are not mentioned in the experimental data [11,13].

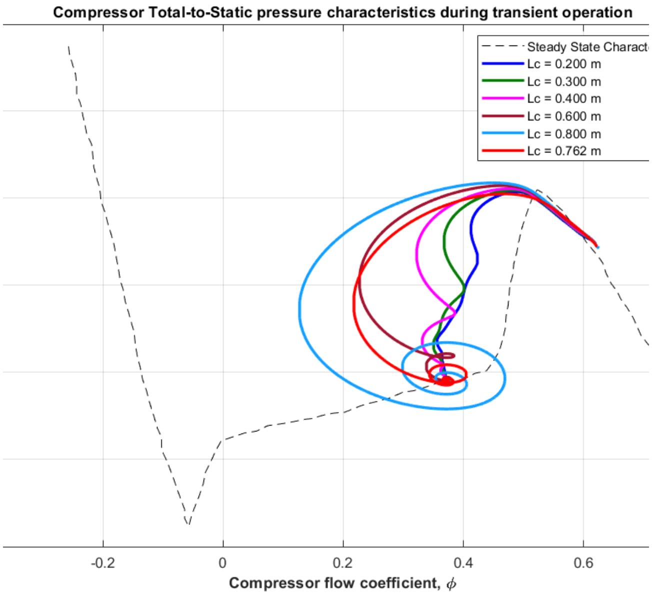

Figure 16 – Effect of Lc and Vp

3.7. Summary and discussion

As a starting point to modelling a PGC based propulsion system, the dynamic model of a multistage, axial compressor is developed. The model is capable of simulating compressor surge and stall and can also simulate interstage bleed as well. The model is validated qualitatively with experimental results and previous models available in the literature. Effect of different parameters on the compressor surge response is also evaluated. Due to the incomplete information of the experimental compression system, the validation of the model had to be limited to qualitative level at certain operating conditions.

DEVELOPMENT OF AIRCRAFT ENGINE MODEL USING TRANSEO

4.1. Introduction

As a part of the research activities, the in-house simulation tool TRANSEO is being used to model a typical aircraft engine (with & without PGC). Application of TRANSEO for simulating aircraft engines has not been done till date. The use of TRANSEO code in modelling an aircraft engine is difficult since the components available in the simulation library are not tailored for aircraft propulsion. The major difficulties arise in the modelling of multistage compressor and turbine, and secondary air system for cooling the combustion chamber and turbines. Hence, modifications are required to accommodate features such as compressor bleed, combustor and turbine cooling and bypass flow. In addition, the tool currently lacks the module to simulate pressure gain combustion, as the existing combustor module is a conventional constant pressure combustion chamber. It is also to be noted that the introduction of a pressure gain combustion chamber warrants additional components as compared to conventional aircraft engines, such as specialized plenum chambers, to mitigate the flow transients from affecting the turbomachinery components.

The current activity focus on developing a conventional aircraft engine with constant pressure combustion and turbine cooling. The model is validated against on-design & off-design performance values available in the public domain. No validation has been possible at the moment on dynamic conditions. The next step is to develop a reduced order dynamic model of the pressure gain combustor and introduce it in the model.

4.2. Literature Review

4.2.1. TRANSEO Simulation Tool

TRANSEO is a MATLAB-Simulink-based simulation tool capable of transient and dynamic simulation of systems, developed by the Thermochemical Power Group, of the University of Genova, Italy. It is designed for simulating systems operating with different cycles and different sizes. It has been successfully employed in the study of microturbine-based energy systems [19,20], and hybrid fuel cell systems[21] and also for supercritical CO_2 cycles [22]. The TRANSEO tool has over 30 built-in modules, along with standardized interconnecting protocols for assembling the modules to obtain the desired system layout. The tool organization is shown in Figure 17.

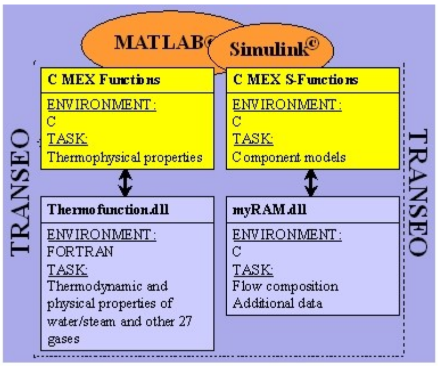

Figure 17 – TRANSEO organization [23]

4.2.2. Aircraft engine modelling

There have been a number of efforts to model the aircraft propulsion systems. This includes, but not limited to, the works by Alexiou [24], Khalil et.al [25], Sankar et. al [26], Carcasci et.al [27,28] Martins [29] and Ridaura [30]. These approaches usually use commercial software like GasTurb or Gas turbine Simulation Program (GSP) to predict the performance of the engine. MATLAB/SIMULINK based tools are also capable of simulating the aircraft engines.

Most of the published works use lumped volume approach for transient simulations. This is where the TRANSEO simulation tool shines, when needed, as it is cable of capturing the effects of internal fluid dynamics as well. Unfortunately, the engine manufacturers are unwilling to provide the detailed geometric and performance data that is required for the dynamic simulation. The data used in this activity has been taken from the literature that is available in the public domain, with reasonable assumptions about the unknown variables.

4.3. Aircraft engine modelling using TRANSEO

The aircraft engine modelled using TRANSEO is a typical high-bypass turbofan engine used in civilian aircrafts. In order to validate the model, CFM56-3 engine manufactured by CFM International is used. The choice of this engine is due to the fact that sufficient amount of data on its performance is available in the public domain. The missing data such as component geometry, heat transfer from components, fuel composition etc. have been approximated to a reasonable value. The model is validated at the on-design & off-design points, where performance data was available, as reported by Ridaura [30].

4.3.1. CFM56-3 Engine

The CFM56-3 engine was developed in the 1970's and has been in service with Boeing 737 as a wing mounted engine till date. It is a 2-spool, high by-pass (5:1) engine, with 3 major versions, as shown in Table 7.

Version	Thrust	Application
CFM56-3B1	89 kN	Boeing 737-300, Boeing 737-500
CFM56-3B2	98 kN	Boeing 737-300, Boeing 737-400
CFM56-3C1	100 kN	Boeing 737-300, Boeing 737-400, Boeing 737-500

Table 7 : Versions of CFM56-3 engine

The details of a typical CFM56-3 engine are given in Table 8.

Engine	CFM56-3
Type	Dual rotor, axial flow, high bypass ratio turbofan
Compressor	1 fan, 3 LP, 9 HP
Combustor	Annular
Turbine	1 HP, 4 LP
Control	Hydro-mechanical + limited electronic
Length	2.364 m
Width	2.018 m
Height	1.817 m
Dry weight	1954–1966 kg
Takeoff thrust	89.41–104.6 kN
Thrust/weight	4.49-5.22
100% spool RPM	LP (N1) – 5179 rpm
	HP (N2) – 14460 rpm
Air flow/sec	289–322 kg
Bypass ratio	5.9-6.0
Max OPR	27.5-30.6
Fan diameter	1.52 m
Takeoff TSFC	10.9–11.2 g/(kN·s)
Cruise TSFC	18.9 g/(kN·s)

Table 8 : Typical CFM56-3 engine details

A typical CFM56-3 engine construction is shown in Figure 18. The single stage high pressure turbine (HPT) drives the 9-stage high pressure compressor (HPC), which rotates at HP spool speed N2. The annular combustion chamber is fed by 20 fuel injectors, which is mixed with the air from the 9th stage of the HPC. The 4-stage low pressure turbine drives the fan and 3 stage low pressure compressor (LPC), rotating at LP spool speed N1. In addition, there are 12 variable bleed valves (VBV) located in the fan structure and between the LPC and HPC to account for the engine transient operation. There are also 4 variable stator vanes (VSV) and 5 outlet guide vanes (OGV) in the HPC. In addition to this, the secondary air-system of the engine is also designed to provide cooling to the HPT & LPT inlet guide vane (IGV) and HPT rotors, and also for the blade tip clearance control (Table 9).

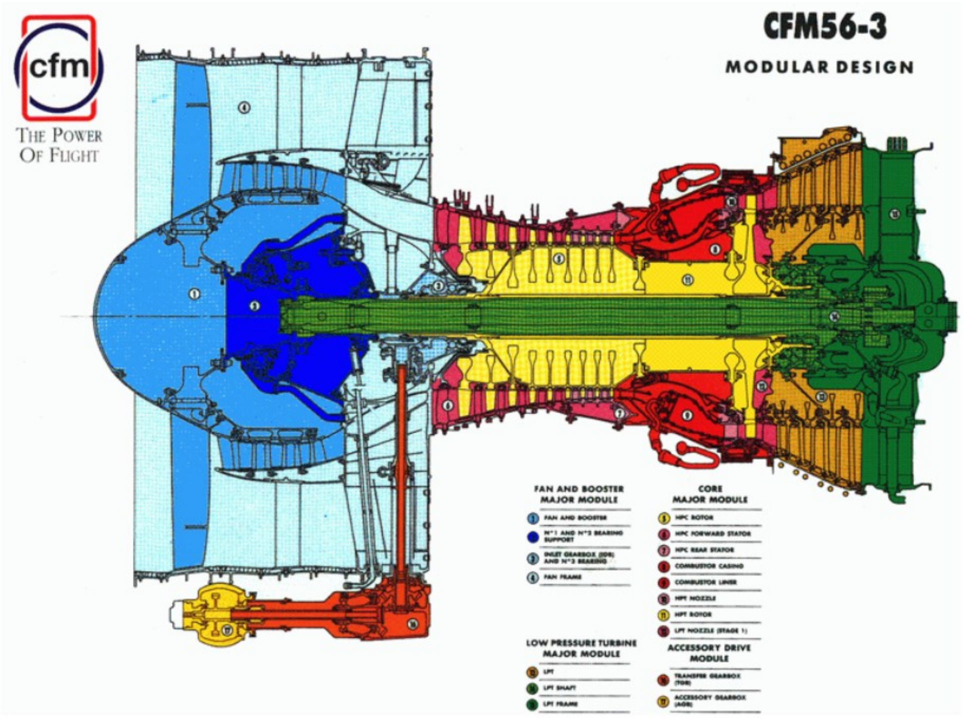

Figure 18 – CFM56-3 Schematic [29]

CFM56-3, CFM56-3B, CFM56-3C		
Bleed location	**LP rotor speed**	**Airflow limit**
Fan discharge	All speeds above 20 % N1K	5 % of secondary airflow
HPC 5th stage only	All speeds above 20 % N1K	10 % of primary airflow
HPC 9th stage only	From 20% to 61 % of N1K	14 % of primary airflow
	From 61 % to 75 % of N1K	Linear variation between 14% and 9,2 % of primary airflow
	Above 75 % of N1K	7% of primary airflow
HPC 5th and 9th stages combined	From 20 % to 61 % of N1K	14 % of primary airflow
	From 61 % to 72,7 % of N1K	Linear variation between 14% and 10% of primary airflow
	Above 72,7 % of N1K	10% of primary airflow

Table 9 : Maximum Permissible Air Bleed Extraction for CFM56 Engine [31]

4.3.2. Engine component geometry and maps

TRANSEO simulation tool requires characteristics maps of the compressor and turbines, along with the areas and lengths of all the components [23]. Unfortunately, this is the proprietary information of the engine manufacturer, and hence not disclosed in public domain. Therefore, for the purpose of modelling the CFM56-3 engine, the maps and other data are taken from approximated values. The maps developed by Ridaura [30] using GasTurb software with modifications specified by Kurzke [32] are used for the on-design validation. Out of the 15 operating points available from the engine test report, the design point chosen is the same as the one used by Ridaura[30], which is close to the maximum spool speed [31]. These maps are adapted to the TRANSEO turbomachinery maps format.

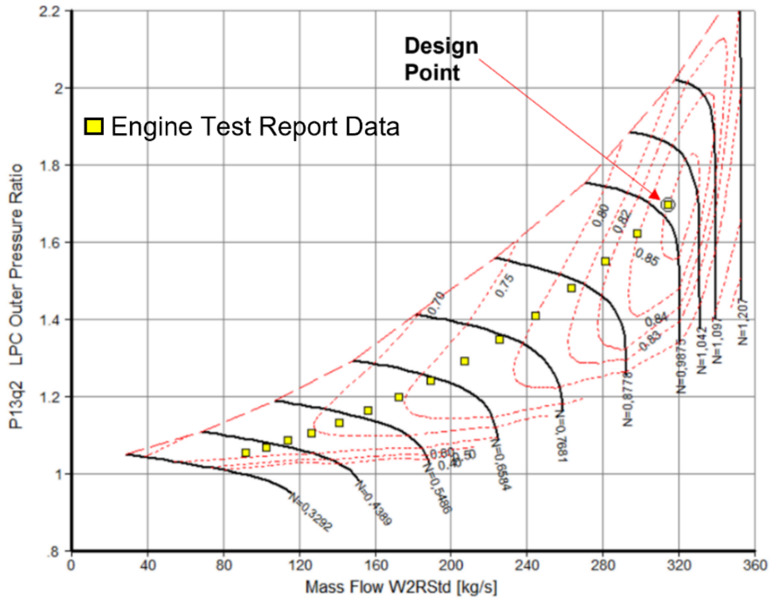

Figure 19 - Fan map with design point [30]

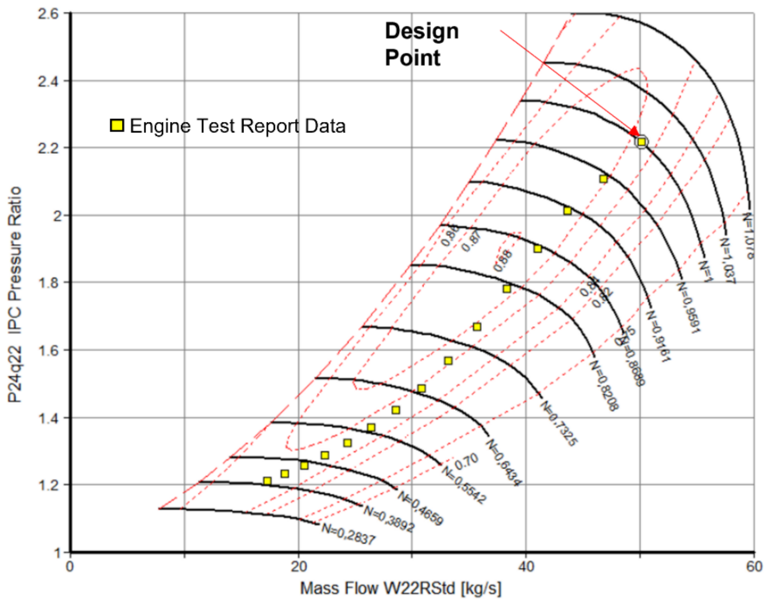

Figure 20 – LPC map with design point [30]

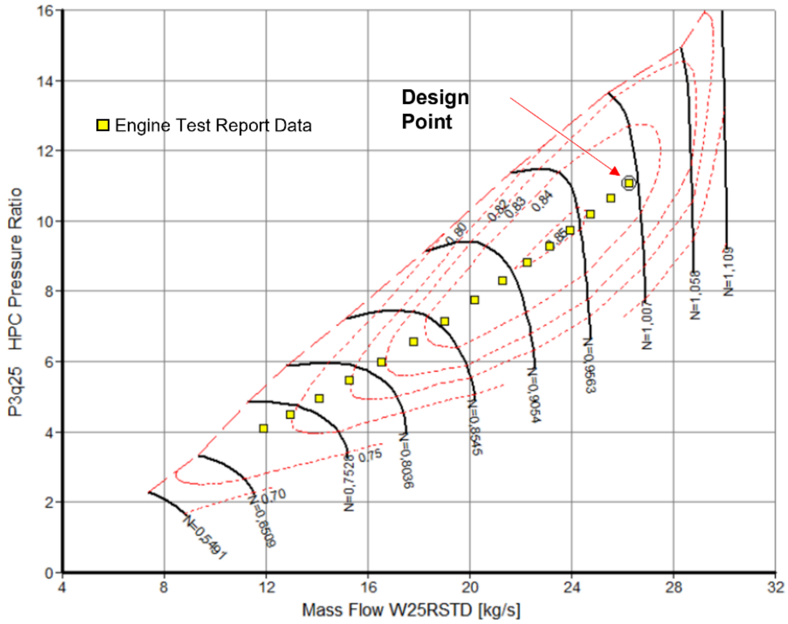

Figure 21 – HPC map with design point [30]

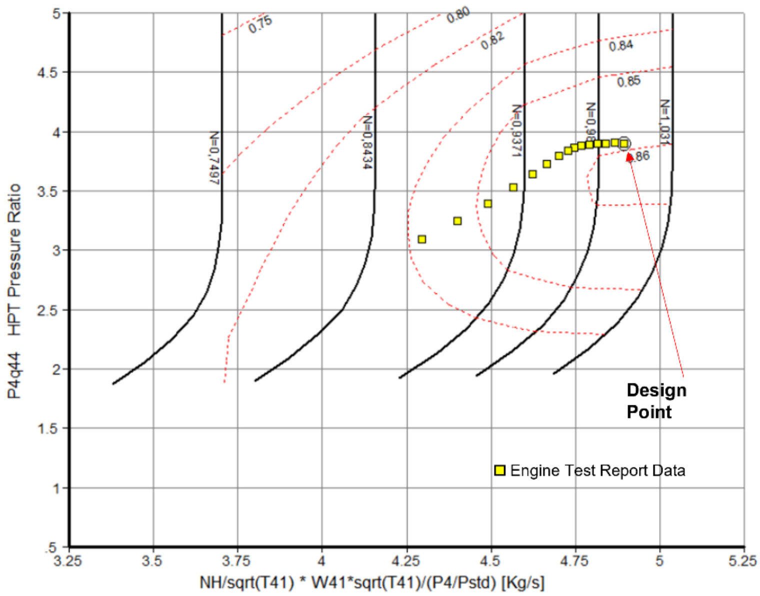

Figure 22 – HPT map with design point [30]

The fan and LPC are modelled using TRANSEO compressor module, while the HPT and LPT are modelled using TRANSEO turbine module. These modules require the pressure ratio v/s corrected mass flow and pressure ratio v/s efficiency maps, along with on-design performance data, heat transfer data and geometry. The maps used for this purpose, along with the design point are shown in Figure 19 - Figure 23.

The station numbering as per SAE convention [33] are shown in Figure 24 and the values of thermodynamic properties at each station are mentioned in Table 10. Since the original engine performance report is not available in public domain, the pressure, temperature, and mass flow rates reported by Ridaura [30] which have been validated against engine performance test data, are used to approximate the engine component areas. The compressor bleed at the design point is taken from Philpot [34] as shown in Table 11. However, the HPT clearance control bleed flow (HPTCC) is not implemented in the simulation, as the TRANSEO model is not configured to account for the rotor blade expansion.

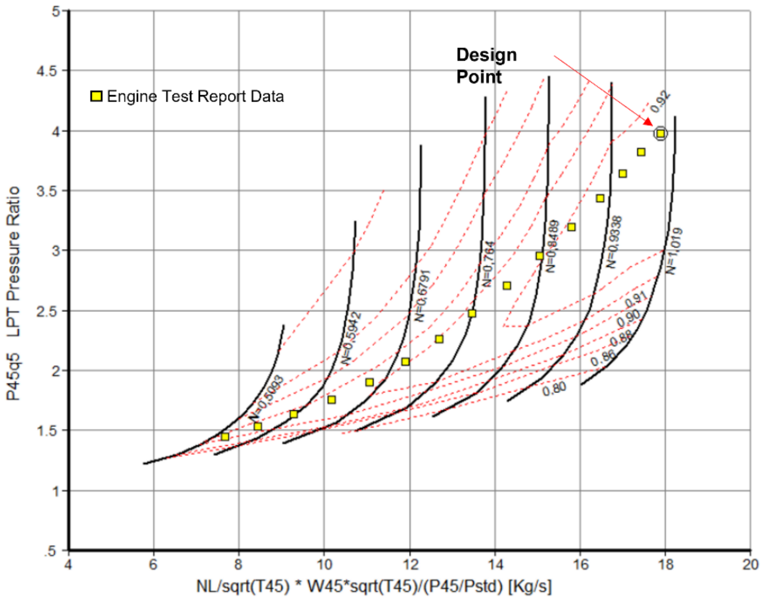

Figure 23 – LPT map with design point [30]

Station	Station Details	Mass Flow (kg/s)	T0 (K)	P0 (Pa)	Area (m^2)
0	Ambient		288.15	101325	
2	Fan intake	314.711	288.15	101325	1.74773
13	bypass duct inlet	264.56	343.271	171887	1.25522
21	core inlet	50.151	288.15	101325	0.4
22	LPC inlet	50.151	288.15	101325	0.4
24	LPC outlet	50.151	372.7	224429	0.375
25	HPC inlet	50.151	372.7	219940	0.38
3	HPC outlet	49.148	786.19	2435887	0.038
31	CC inlet	43.632	786.19	2435887	0.038
4	CC outlet	44.7256	1629.48	2314092	0.04
41	HPT inlet	47.735	1580.77	2314092	0.405
44	HPT outlet	50.2423	1195.84	593945	0.405
45	LPT inlet	51.2453	1185.22	588006	0.41
5	LPT outlet	51.2453	872.89	148036	0.3
8	core nozzle outlet	51.2453	872.89	146555	0.2933
18	bypass nozzle outlet	264.56	343.27	167590	0.7352

Table 10 : Engine geometry and thermodynamic properties at different stations

The engine tests were conducted on the ground test facility, therefore the flight velocity or V_flight is considered as zero.

CFM56-3 Internal Air System		
Description	**Mass flow (%)**	**Point of extraction**
HPTCC	10	Booster discharge
NGVs HPT	6	Ninth HPC stage
Rotor HPT	5	Ninth HPC stage
NGVs LPT	2	Fifth HPC stage

Table 11 : CFM56-3 Internal air system configuration at design point [34]

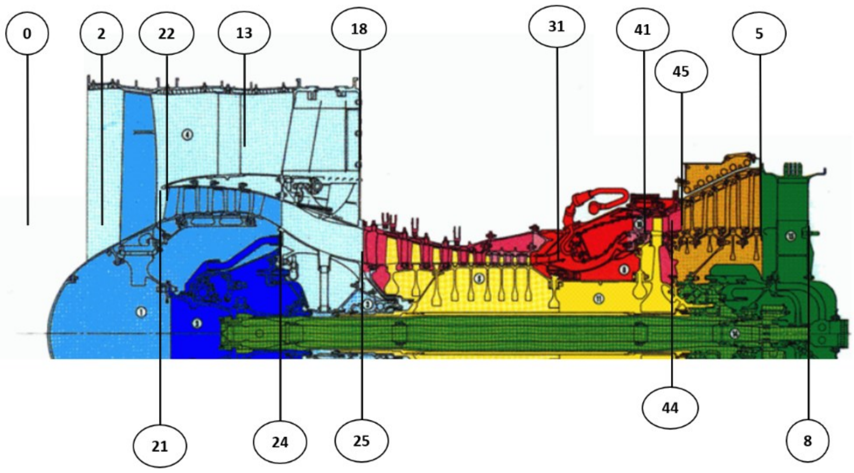

Figure 24 – SAE station numbering convention [30]

4.3.3. Engine model and component description

The CFM56-3 engine is modelled in TRANSEO as shown in Figure 25 and Figure 26. The two models differ from each other in the methodology adopted for modelling the turbine cooling. Since this activity is meant to demonstrate the methodology & capability of TRANSEO to model an aircraft engine, the model represented here is valid for on-design condition. Although, this can be adapted to off-design conditions as well, with minor modifications.

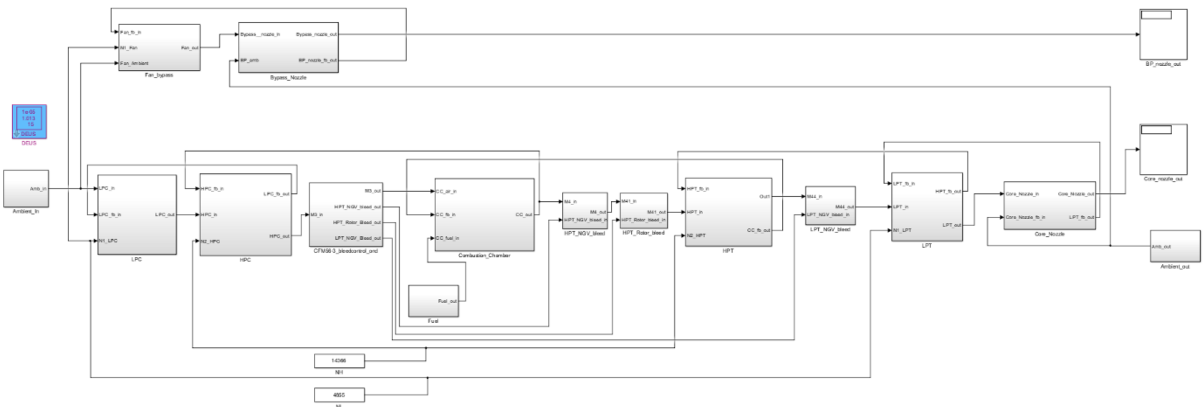

Figure 25 – CFM56-3 model (Type – 1) in TRANSEO (design-point)

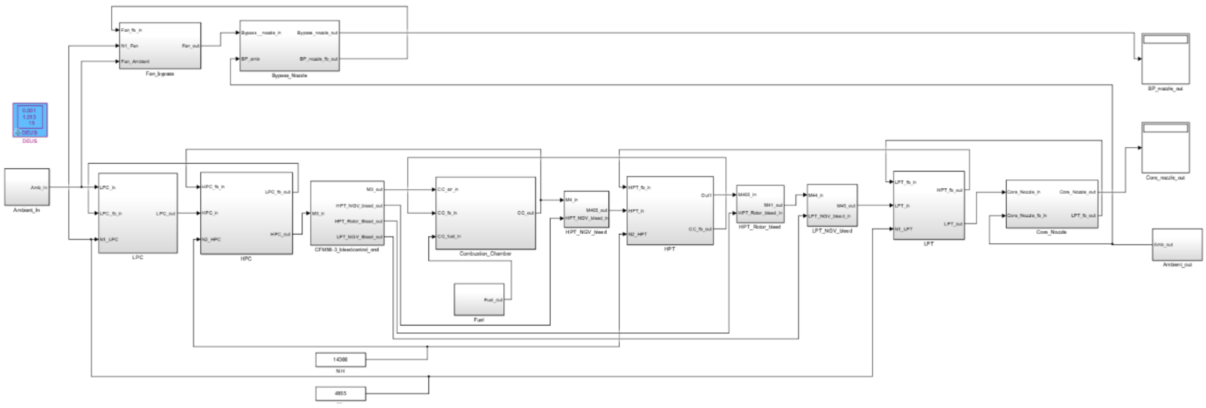

Figure 26 – CFM56-3 model (Type – 2) in TRANSEO (design-point)

4.3.3.1. Ambient_in

This component is used to specify the air inlet conditions. Since the validation is done on engine performance at sea level (ground test conditions), standard day sea level conditions of 101325 Pa and 288.15 K are considered as the inlet conditions. The properties of air at this condition are also included in the component, as shown in Figure 27.

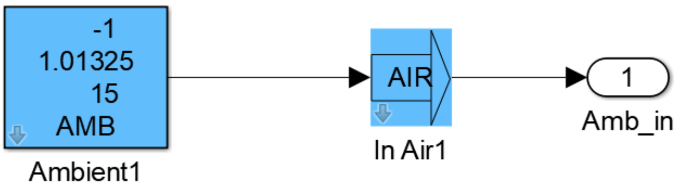

Figure 27 – Ambient_in component

4.3.3.2. Fan_bypass

This component is used to model the primary air-system in the Fan – bypass path (Figure 28). The compressor component is provided with the corresponding maps, the ambient air inlet conditions and the N1 rpm. The heat transfer is approximated, as it was not available in the literature.

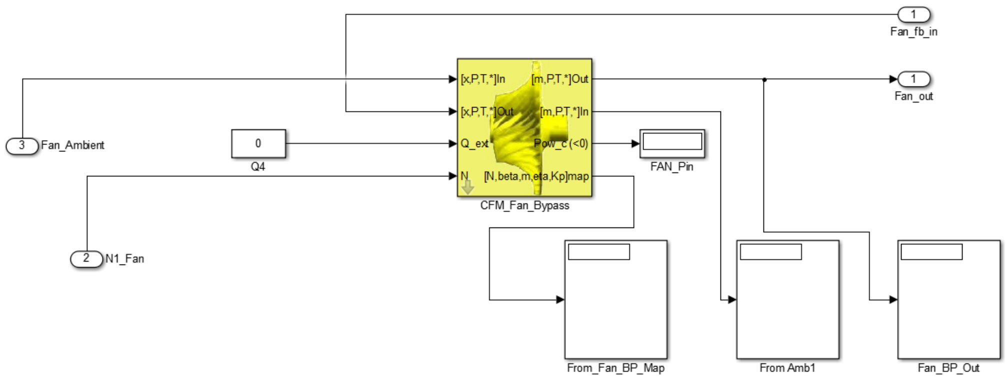

Figure 28 – Fan_bypass component

4.3.3.3. Bypass_Nozzle

This component is used to model the bypass nozzle/cold nozzle of the CFM56-3 engine (Figure 29). The nozzle throat area (A18) was specified as 0.7352 m^2 in the performance test report, and hence is a fixed geometric parameter. The nozzle efficiency is estimated as 0.9553 at on-design point from the test report data.

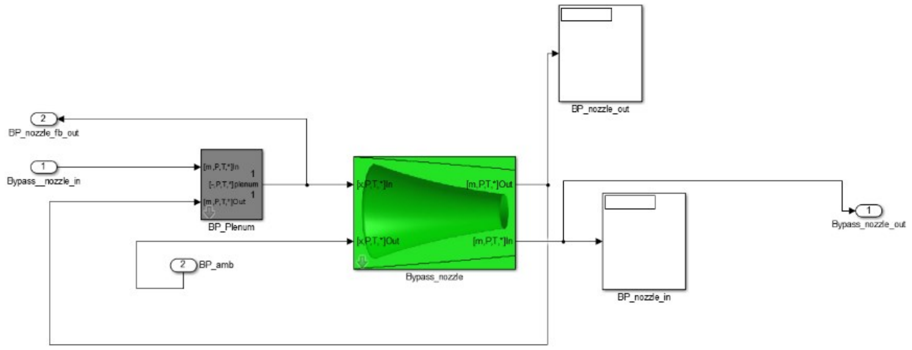

Figure 29 – Bypass_Nozzle component

4.3.3.4. LPC

This component is used to model the low-pressure compressor (Figure 30). The maps are modified according to the TRANSEO format, and the on-design conditions are specified as well. The heat transfer from the compressor and the ambient is approximated since this data was not available in the literature.

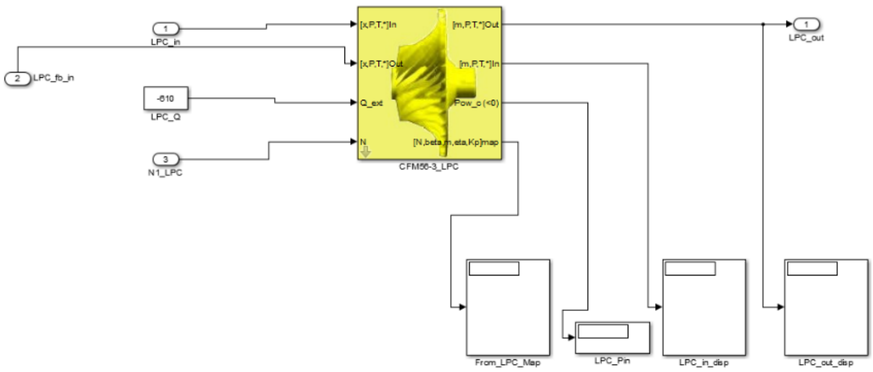

Figure 30 – LPC component

4.3.3.5. HPC

This component is used to model the high-pressure compressor (Figure 31). The maps and on-design conditions are provided to the component in TRANSEO format. The bleed air is assumed to be taken from the compressor outlet rather than interstage locations, since TRANSEO compressor module is yet to be modified for such purpose. It should be noted that individual stage performance maps and compressor stage geometry is often required to simulate the interstage bleed, which is usually not available in public domain. Once again, the heat transfer with the ambient is approximated.

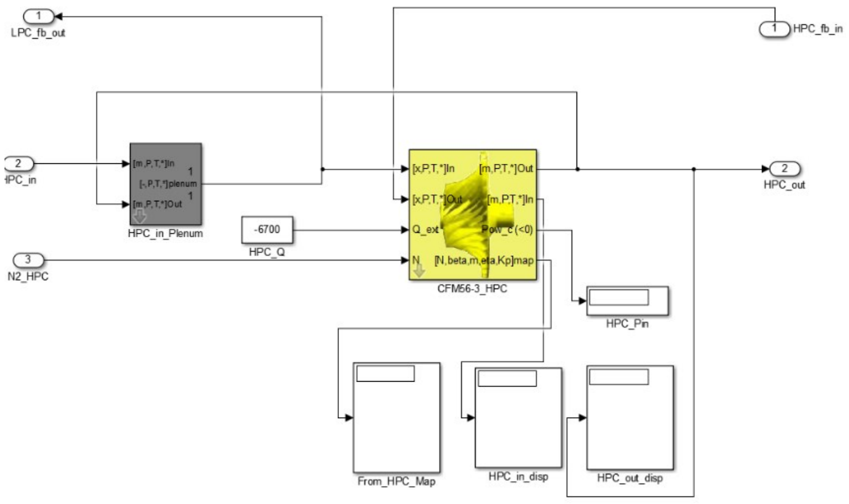

Figure 31 – HPC component

4.3.3.6. Fuel

This component is used to model the fuel supply system of the engine (Figure 32). TRANSEO library contains many gaseous fuel species and can generate blended fuels as well. But for the purpose of simulating the on-design combustion process, a generic fuel was selected having a heating value of 43.8 MJ/kg as mentioned in the thesis of Ridaura [30]. One of the disadvantages of this is the miscalculation of species in the combustion products. The fuel flow rate is also kept the same as in literature.

4.3.3.7. Bleed Control

The bleed control/scheduler is used to extract the mass flow and enthalpy from the HPC outlet. In on-design condition, where the bleed flow is specified, the control is a simple mass flow redistribution and enthalpy balancing, as in Table 11 (Figure 33). For the off-design condition a detailed version of the schedule as a function of the spool speed is required. Unfortunately, the engine manufacturers do not provide this value explicitly and the data available from engine certification agencies, such as in Table 9, do not specify the details such as compressor bleed-off and bleed delivery line geometries. Therefore, the data available at high operating speeds (Table 11) are assumed to hold same at off-design conditions as well.

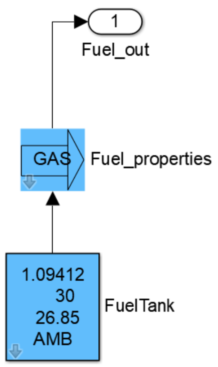

Figure 32 – Fuel

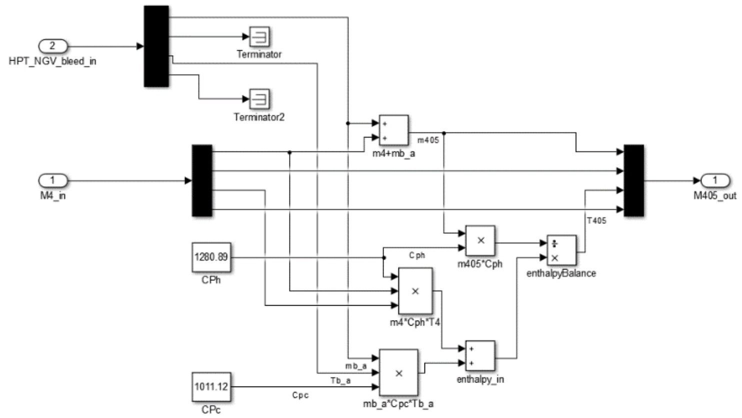

Figure 33 – Typical on-design bleed delivery control

4.3.3.8. Combustion Chamber

This component is used to model the conventional combustion chambers of the CFM56-3 engine (Figure 34), with pressure drop. The fuel and compressed air are the major inputs to the model. The pressure loss across the combustor at on-design condition is approximated along with the heat transfer parameters. The component also requires a minimum fuel-to-air pressure ratio and minimum heat release rate, which determine if the combustion process lights on or not.

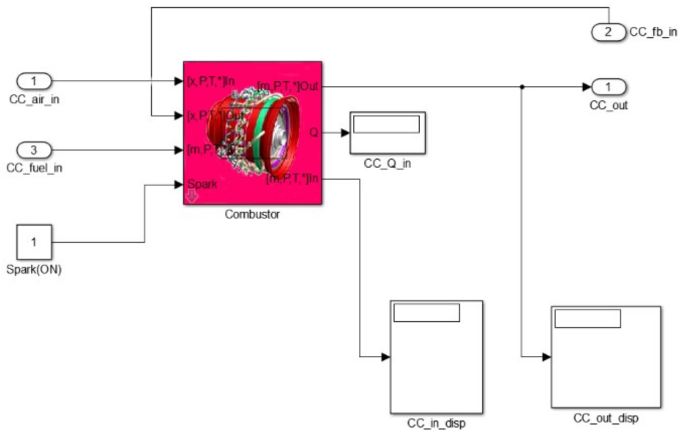

Figure 34 – Combustion chamber component

4.3.3.9. HPT

This component is used to model the high-pressure turbine (Figure 35). Similar to the compressors, the turbine module also requires maps and on-design data. Since blade cooling is not yet implemented in TRANSEO, the cooling flow for the HPT NGVs and rotors are supplied as shown in Type-1 (Figure 25) and Type-2 (Figure 26) models to determine the method that closely resembles the engine test report. This is done, since in usual practice, the cooling flow is assumed to mix in a plenum upstream of the relevant turbine stage, and stage isentropic efficiency is adjusted to obtain the same stage exit temperature. The heat exchange between the turbine and the ambient are also approximated.

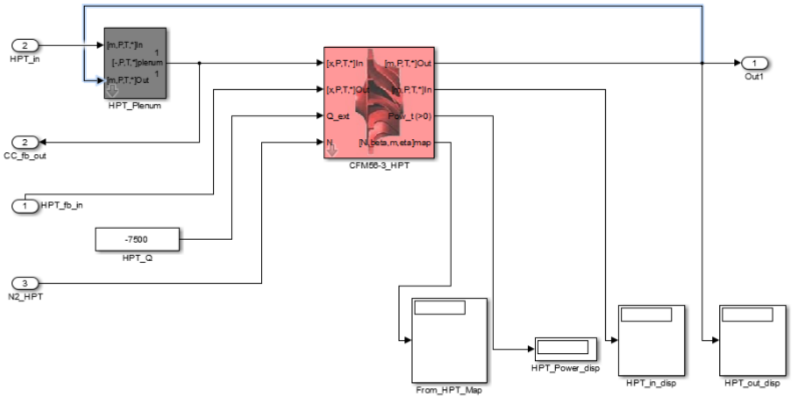

Figure 35 – HPT component

4.3.3.10. LPT

This component is used to model the low-pressure turbine (Figure 36). The LPT NGV cooling flow is supplied upstream of the turbine plenum for the same reason as mentioned in the case of HPT component. The maps and on-design conditions are provided to the turbine module in the TRANSEO format. The heat exchange is also approximated.

4.3.3.11. Core Nozzle

This component is used to model core nozzle/hot nozzle (Figure 37). The nozzle throat area (A8) was specified as 0.2933 m^2 in the performance test report, and hence is a fixed geometric parameter. The nozzle efficiency is estimated as 0.9553 at on-design point from the test report data.

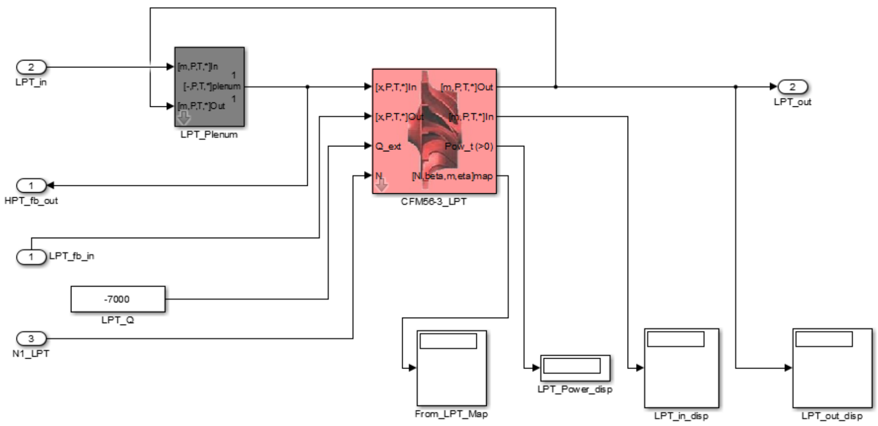

Figure 36 – LPT component

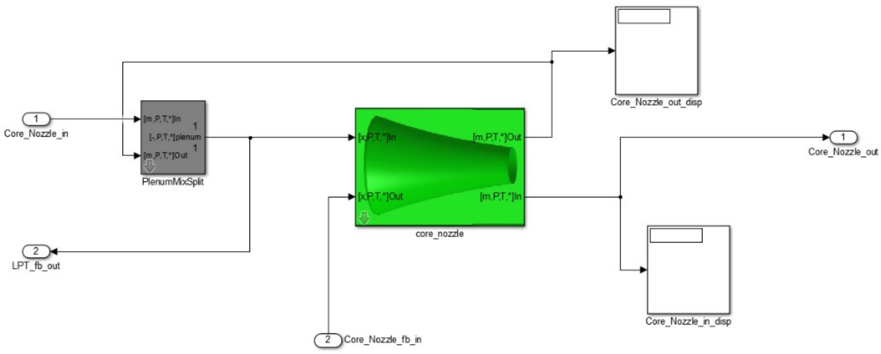

Figure 37 – Core_Nozzle component

4.3.3.12. Ambient out

This component is used to specify the outlet air conditions (Figure 38). Since the validation is done on engine performance at sea level, standard day sea level conditions of 101325 Pa and 288.15 K are considered as the outlet. This condition is used to determine if the nozzles are choked or not, and therefore an important parameter in the calculation of thrust.

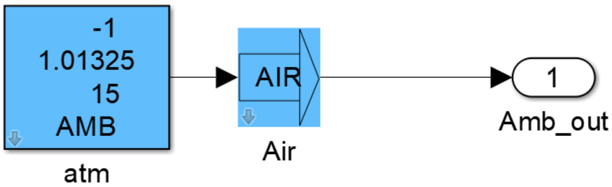

Figure 38 – Ambient_out component

4.4. On-design simulation results & discussion

The model developed using the TRANSEO simulation tool is run in SIMULINK to obtain convergence in steady state on-design conditions. Since the operational parameters for the simulation is same as on-design parameters, the simulation converges into steady-state quickly, as shown in Figure 39.

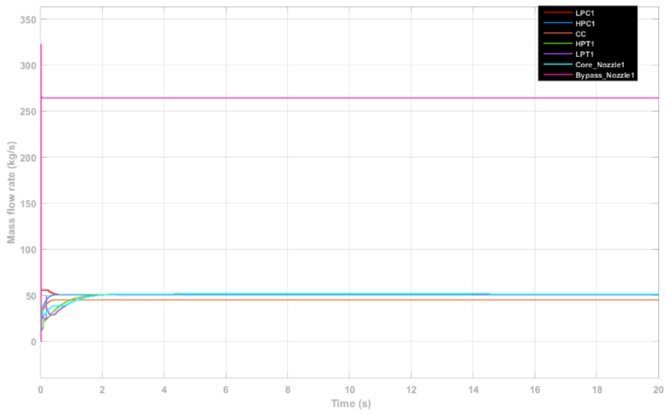

Figure 39 – On-design simulation progress

There are two models that are developed in TRANSEO to closely represent the engine model, as shown in Figure 25 (Type-1) & Figure 26 (Type-2). These two models were checked against the on-design engine test report values from Ridaura [30], to identify the one that closely represents HPT cooling. The variation of mass flow rate, total temperature, and total pressure at each station (as per Figure 24) between the engine test report and the values obtained from the TRANSEO simulation are as follows. The variation is calculated as in equation 4.1.

$$\%\, \boldsymbol{variation} = \mathbf{100} \text{ x } (\boldsymbol{Model} - \boldsymbol{Test\ report})/\boldsymbol{Test\ report} \qquad (4.1)$$

In Type-1, the HPT NGV and HPT rotor blade cooling air is provided upstream of HPT component while LPT NGV cooling air is provided upstream of LPT component, as shown in Figure 40. Both the mass flow and enthalpies are balanced inside the bleed delivery control. The difference in the thermodynamic properties along the gas path are shown in Table 15 and Figure 41.

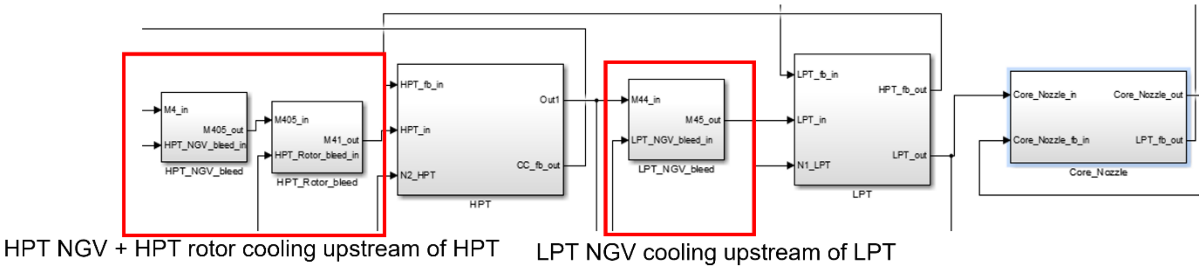

Figure 40 – Cooling methodology for Type-1 model

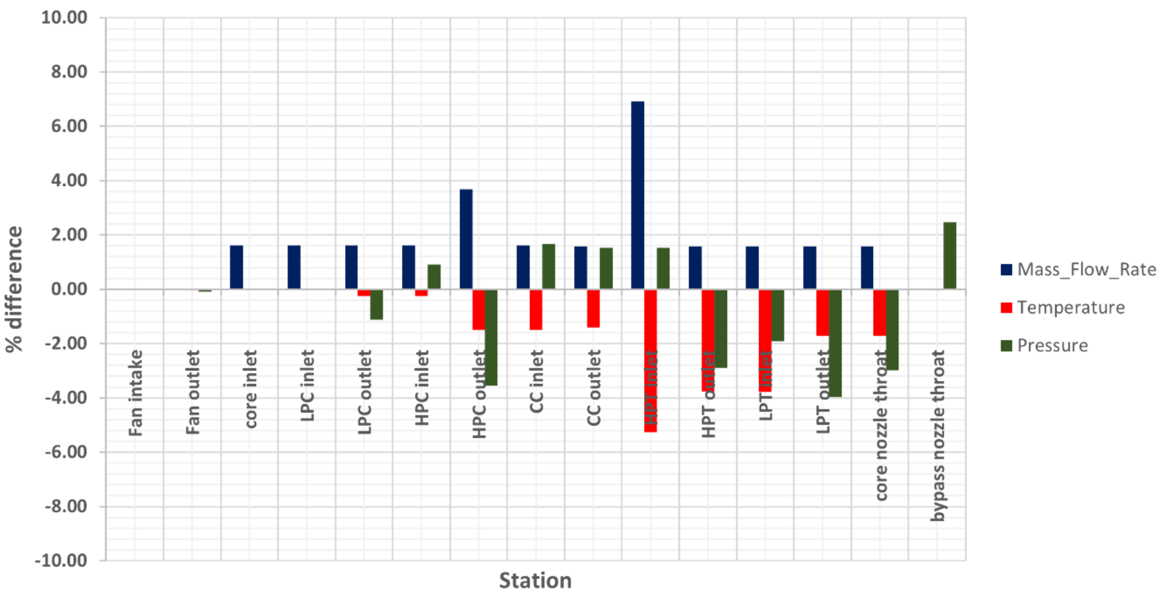

Figure 41 - Variation of thermodynamic properties for Type-1 model

In Type-2, the HPT NGV cooling air is provided upstream of HPT component, while the HPT rotor cooling air and LPT NGV cooling air supplies are provided between the HPT and LPT components, as shown in Figure 42. The variation in the thermodynamic properties is shown in Table 16 and Figure 41.

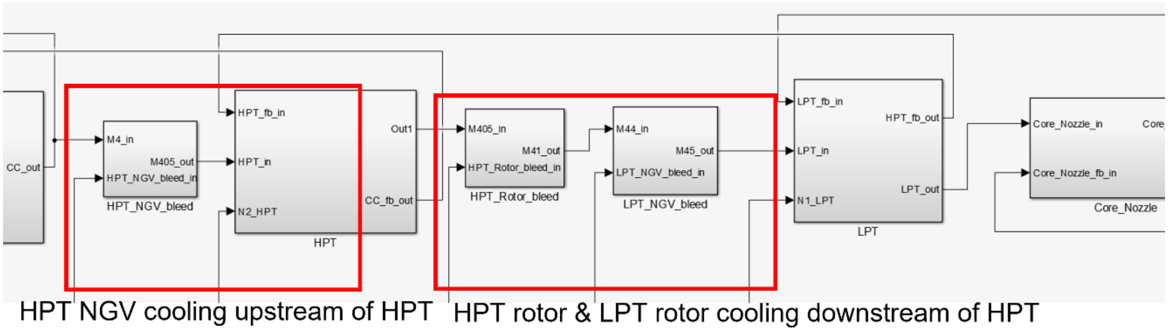

Figure 42 – Cooling methodology for Type-2 model

It can be seen from the results that the maximum variation in mass flow rate occurs at HPT inlet for Type -1 and HPT outlet for Type -2. For the total temperature, this location is HPT inlet for Type-1 while it is at LPT inlet for Type-2. And for total pressure, the maximum variation is found at LPT outlet for Type-1, while for Type-2, it is at HPC outlet. This difference can be attributed to the fact that the injection of bleed air into the HPT, and the subsequent increase in mass flow rate and decrease in temperature, results in a significant change of inlet conditions of the turbine. Therefore, the HPT overpredicts/underpredicts the efficiency and pressure ratio from the maps, and this results in a different output from the turbine module calculations. This output affects the LPT calculations as well, resulting in a variation in the properties upstream and downstream of both turbine components, offsetting the entire gas path from the design point.

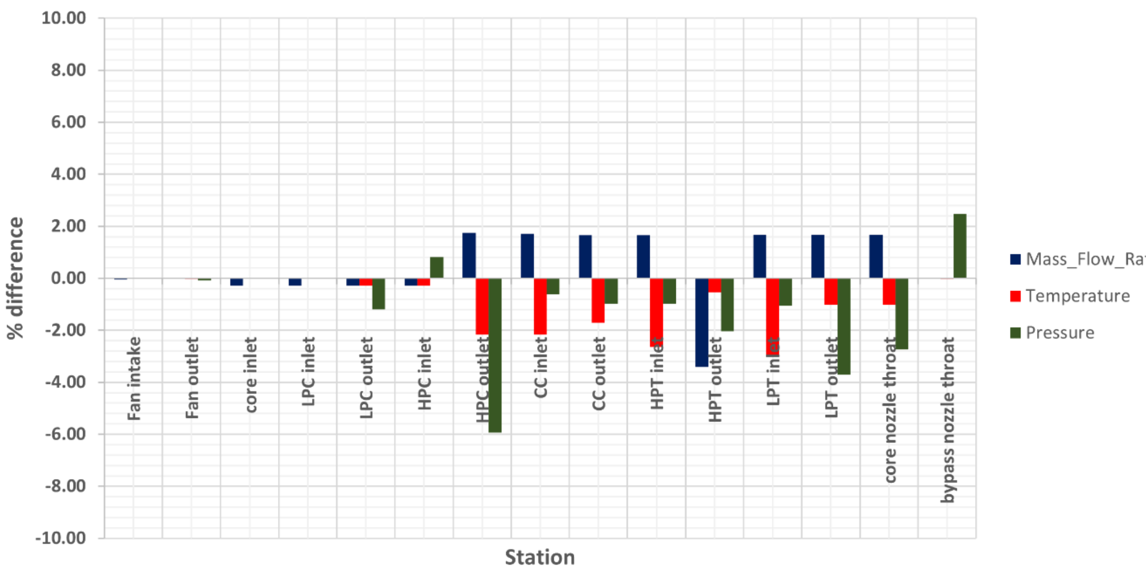

Figure 43 - Variation of thermodynamic properties for Type-2 model

To clearly understand the effect this has on the engine performance, the net thrust and the thrust specific fuel consumption (TFSC) and calculated for both models. For this purpose,, the values of P_8, P_{18}, T_8, T_{18}, $\dot{m}_8$ and $\dot{m}_{18}$ are retrieved from the TRANSEO simulation. These values are used to calculate the net thrust generated and TSFC for the engine using the method given in Chapter 3 of [35], and as explained briefly in Appendix 2.

The calculations yield the following results for thrust and TSFC for Type-1 & Type-2.

Parameter	Performance Test Report	TRANSEO simulation	% Difference
Net Thrust (kN)	99.65	100.68	1.033 %
TSFC (g/kN-s)	10.98	10.8674	-1.018%

Table 12 – Comparison of results for Type -1

Parameter	Performance Test Report	TRANSEO simulation	% Difference
Net Thrust (kN)	99.65	100.85	1.205 %
TSFC (g/kN-s)	10.98	10.8489	-1.186%

Table 13 – Comparison of results for Type -2

From the results obtained, it is clear that the inner errors in temperatures and pressures are mitigated at system level, where overall thrust and TSFC are very well predicted. However, considering also the gas path details, it can be concluded that Type-2 model is better suited to represent this type of engine using the TRANSEO modules available currently. The small penalties in the performance prediction as compared to Type-1 model can be justified when the variations in the gas path predictions are taken into account.

The variation in the results could also be partly attributed to the unavailable data on heat exchanges, the accuracy in the component maps and geometry, the detailed secondary air system including interstage bleed and NGV/rotor cooling, and the uncertainties in the measurements from the engine test bed. Further studies will be aimed at improving these factors allowing the TRANSEO library to model the engine components more accurately.

4.5. Off-design simulation results & discussion

The Type-2 model is subjected to off-design simulations using the data available from Ridaura [30]. This is done by introducing the shaft component of TRANSEO into the Type-2 model. The shaft component (Figure 44) simulates the dynamic behaviour of a rotating spool through the balancing of the compressor and turbine powers [23].

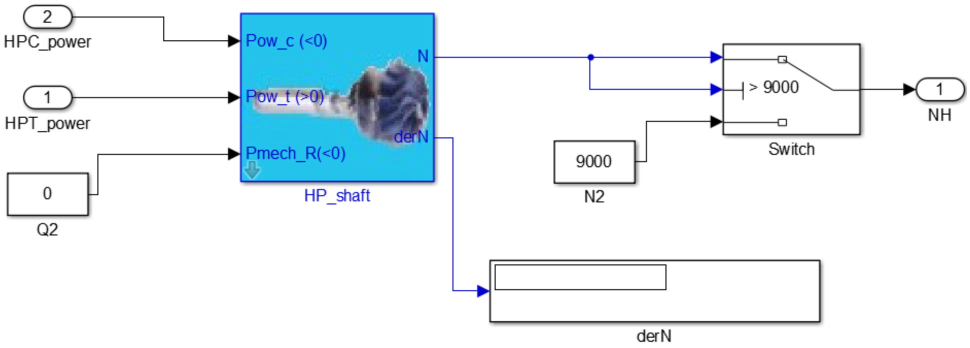

Figure 44 – Shaft component

The shaft component uses an approximate spool speed at the start of the simulation for numerical stability (provided by the user), and once the speed satisfies a threshold value, the component delivers the calculated speed to the turbomachinery in the spool. The simulation is terminated when the change in the shaft speed is negligible.

To validate the simulation with engine test report, the fuel flow rate from the TSFC v/s Net Thrust graph provided in Ridaura [30] is used in the fuel component (Figure 32) as shown in Table 14. All other components are left to operate as per the model dynamics of TRANSEO. The results of the off-design simulation are presented in Figure 45 to Figure 57 and in Table 14. To define the exhaust gas temperature (EGT) the following experimental function (Eq. 4.12), which is suited for the CFM56 engine family, is employed [30,32].

$$\boldsymbol{EGT = 0.967 \times (T45 - 0.27 \times (T45 - T5))} \qquad (4.12)$$

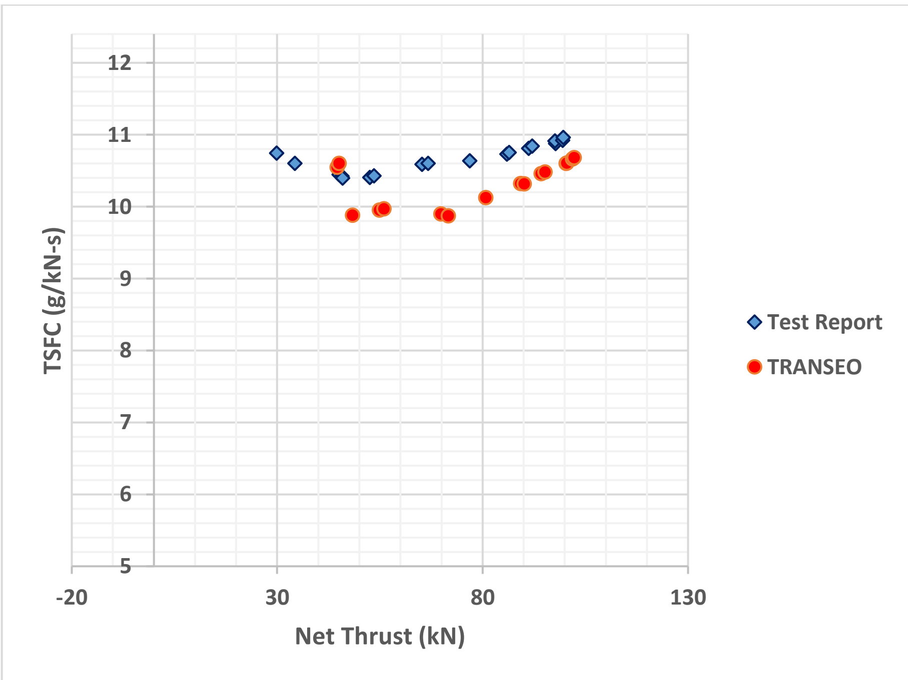

Figure 45 – Net Thrust v/s TSFC

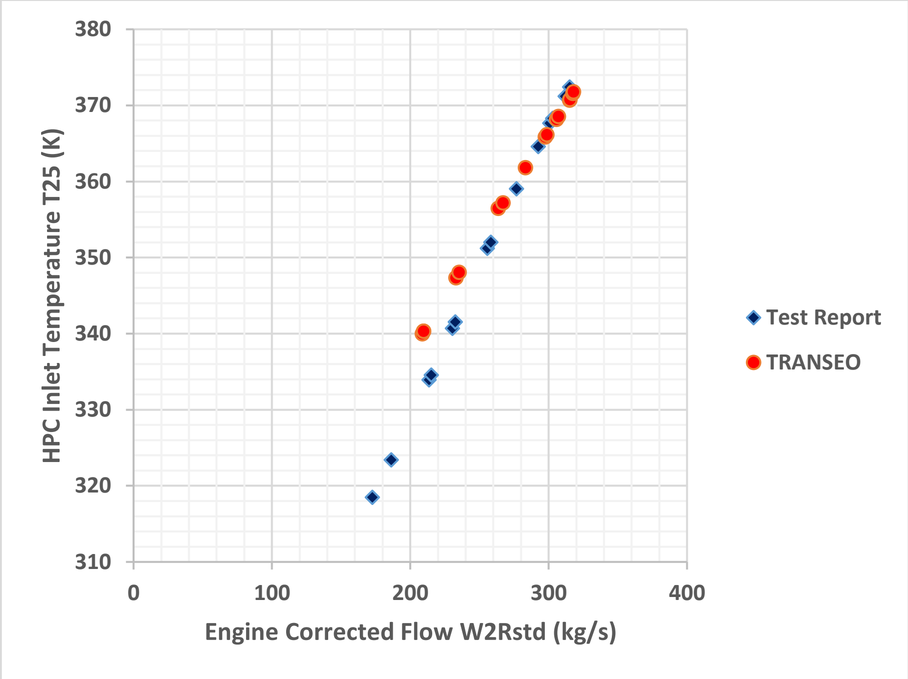

Figure 46 – HPC inlet temperature

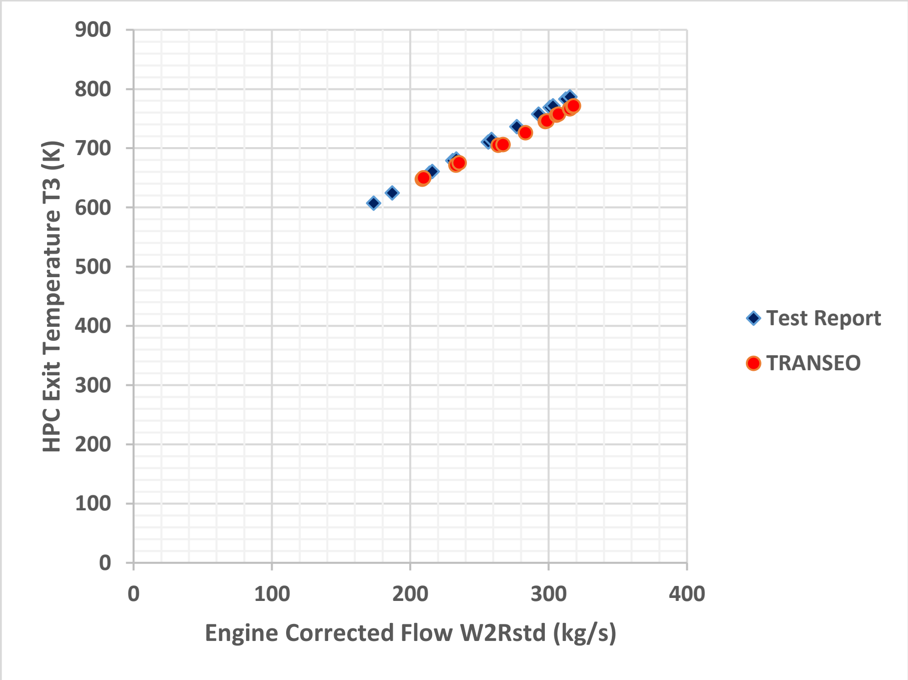

Figure 47 – HPC exit temperature

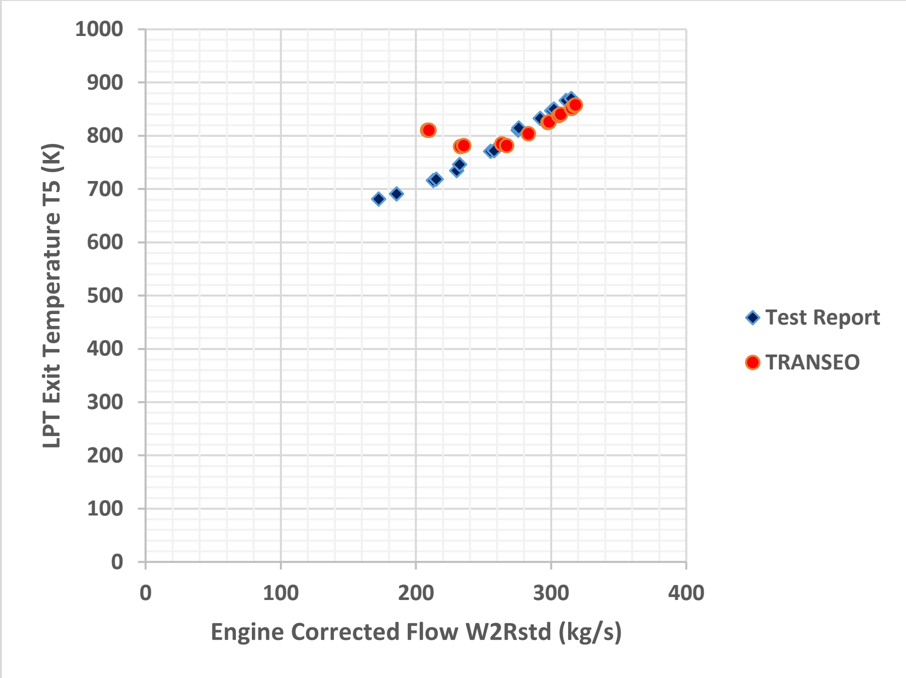

Figure 48 – LPT exit temperature

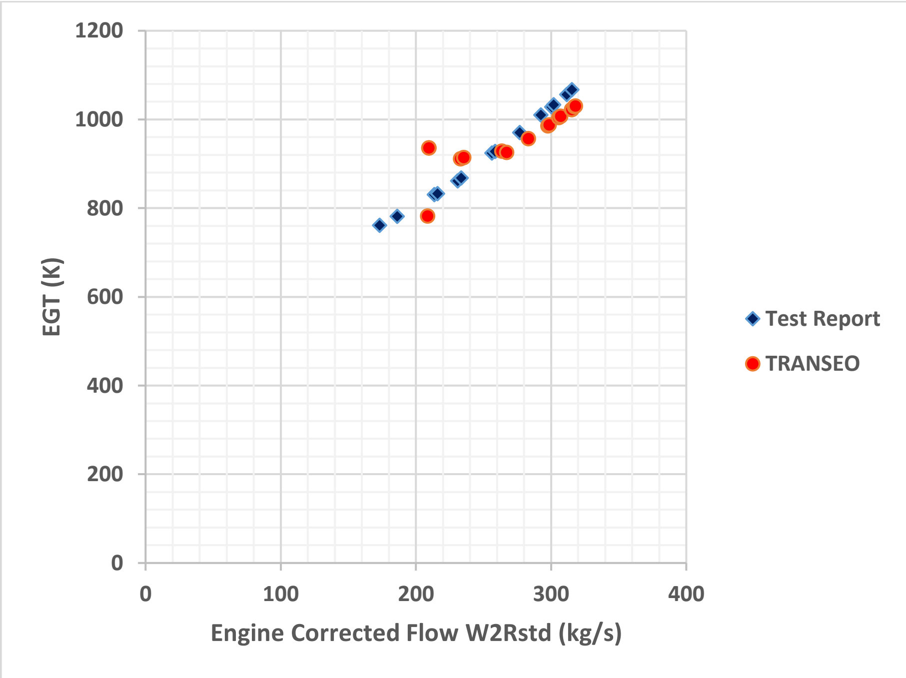

Figure 49 – Exhaust gas temperature

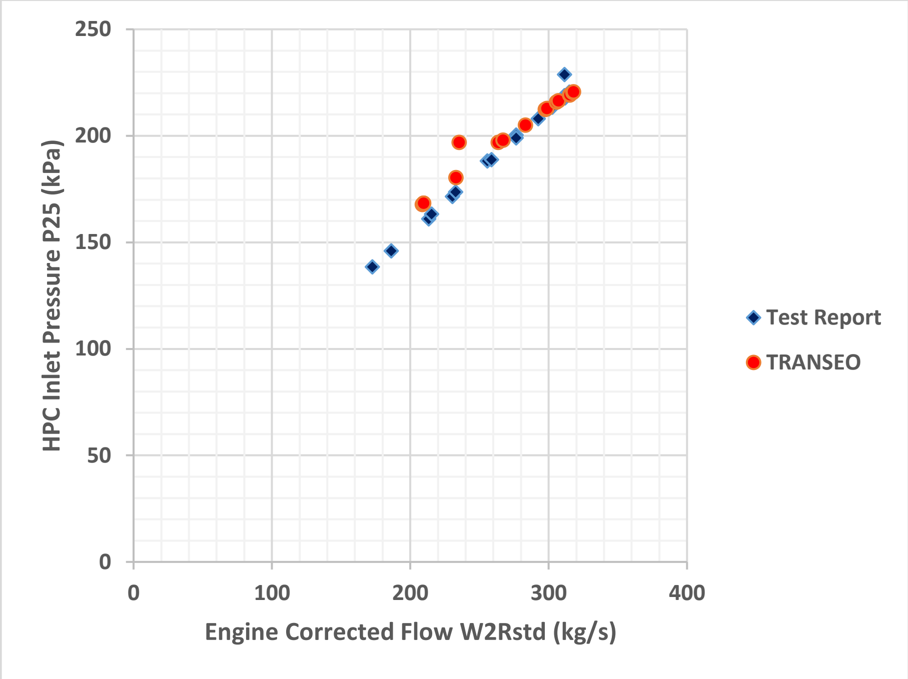

Figure 50 – HPC inlet pressure

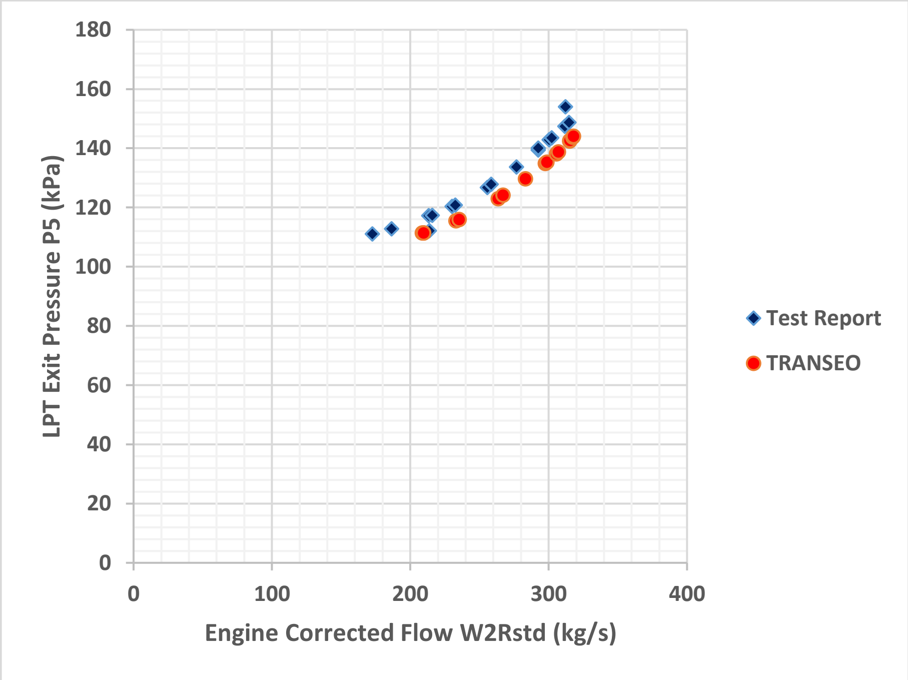

Figure 51 – LPT exit pressure

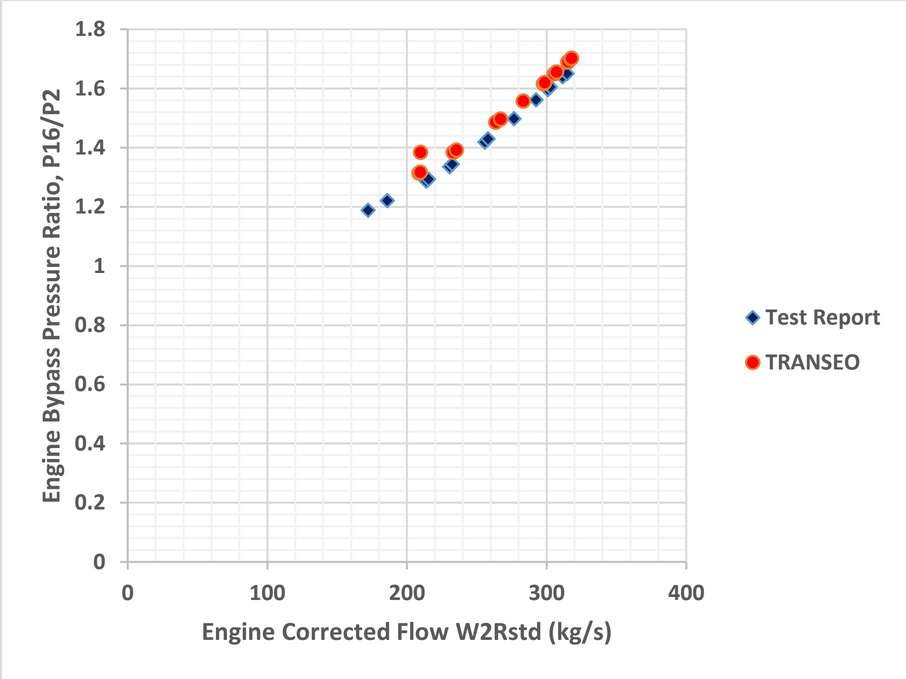

Figure 52 – Engine bypass pressure ratio (P16/P2)

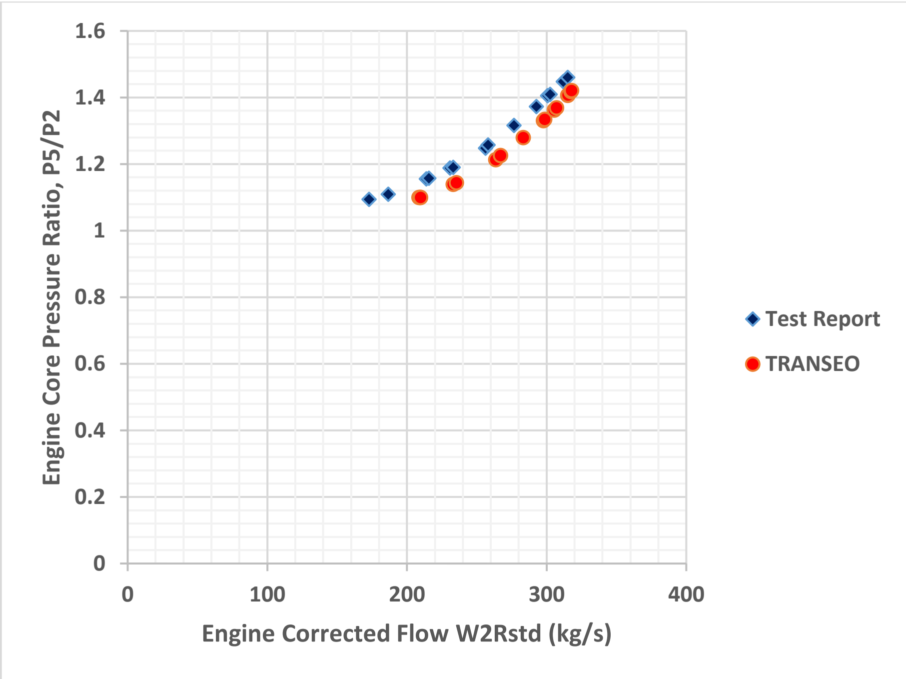

Figure 53 – Engine core pressure ratio (P5/P2)

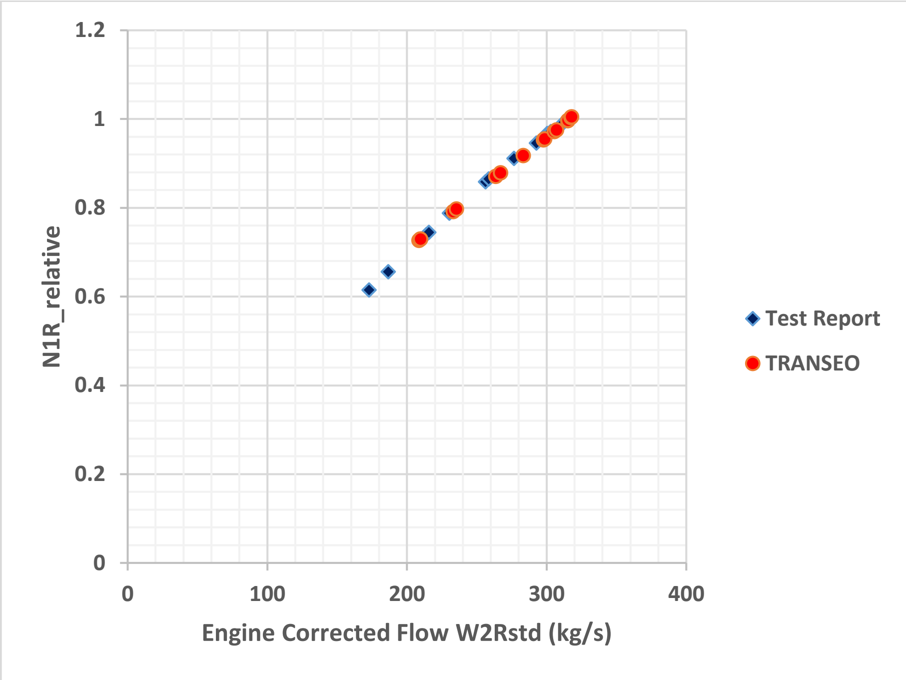

Figure 54 – Corrected relative low pressure spool speed

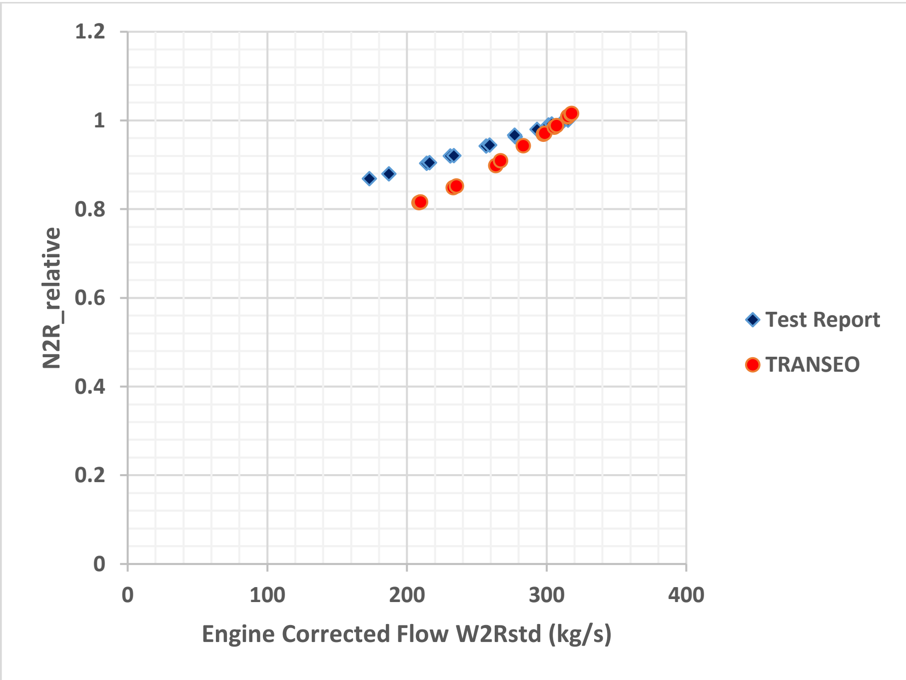

Figure 55 - Corrected relative high pressure spool speed

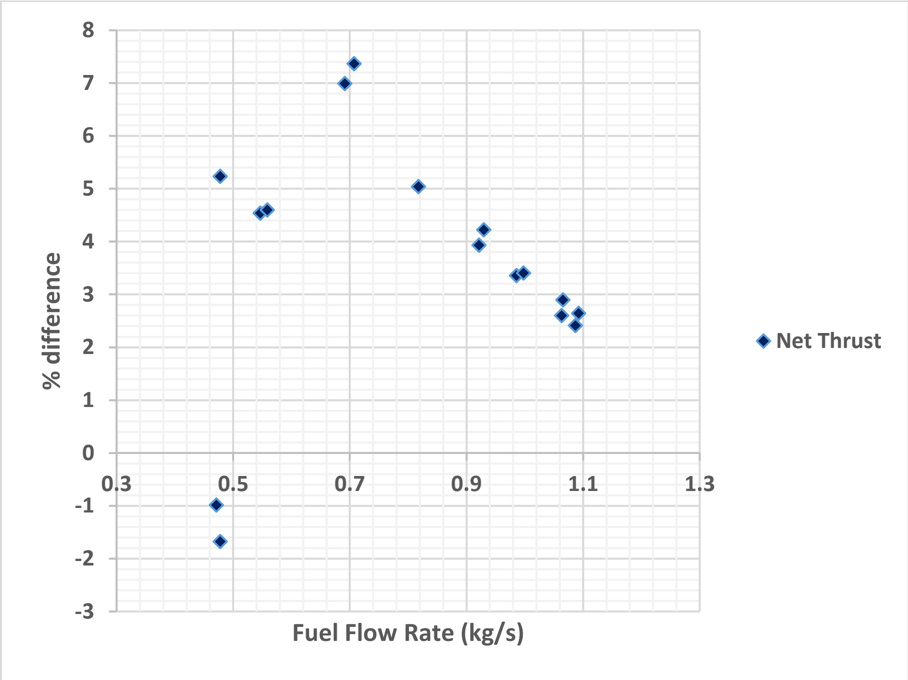

Figure 56 - Variation of net thrust

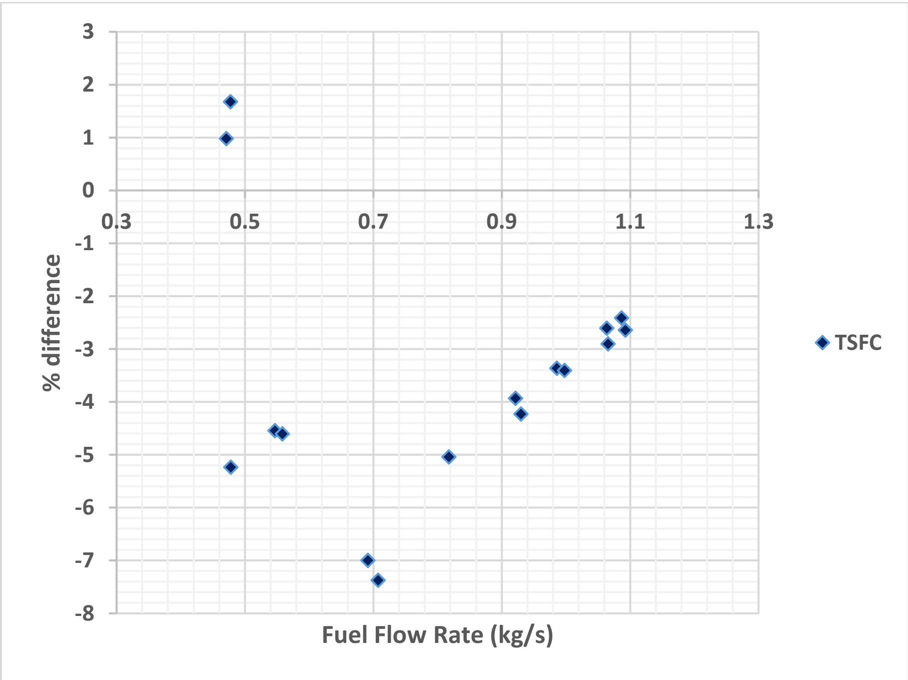

Figure 57 – Variation of TSFC

As evident from the temperatures and pressures along the gas path shown in Figure 46 to Figure 53, the TRANSEO model predictions are close to the engine test report values. The percentage variations in net thrust (Figure 56) and TSFC (Figure 57) are also reasonably within acceptable values for most of the case. The net thrust v/s TSFC is also very close to each other for medium to high mass flow rates.

Test No	Fuel flow rate	Net Thrust	TSFC	P5/P2	P16/P2	T25	P25	T3	T5	P5	W2	Corr. Rel. N1	Corr. Rel. N2	EGT
	kg/s	kN	g/kN-s			K	kPa	K	K	kPa	kg/s			K
1	0.471138	44.66	10.54949	1.099704	1.31414	340.00	167.86	647.88	810.87	111.43	208.68	0.726797	0.8143464	782.5018
2	0.477663	45.05	10.60255	1.099704	1.317165	340.34	168.38	649.84	810.87	111.43	209.66	0.729763	0.8162258	935.5643
3	0.477821	48.37	9.878579	1.099741	1.385245	340.34	168.38	649.88	810.93	111.43	209.73	0.729804	0.8162676	935.6432
4	0.546696	54.94	9.951468	1.139481	1.385245	347.38	180.48	671.73	780.27	115.46	233.11	0.792008	0.8487679	911.0956
5	0.55845	56.02	9.969309	1.144253	1.392637	348.07	196.92	675.22	781.97	115.94	235.39	0.797899	0.8522066	914.2334
6	0.691372	69.86	9.896504	1.213583	1.486007	356.48	196.92	705.34	785.15	122.97	263.67	0.871287	0.8984408	928.7288
7	0.707354	71.64	9.873422	1.225681	1.496891	357.21	197.99	706.36	782.16	124.19	267.16	0.879423	0.9087916	925.8801
8	0.817918	80.77	10.12689	1.279331	1.557749	361.84	205.12	726.23	804.42	129.63	283.35	0.918373	0.9427844	956.8561
9	0.921633	89.29	10.3217	1.330707	1.615932	365.89	212.43	745.06	824.92	134.83	297.69	0.953223	0.9692399	985.7335
10	0.929924	90.14	10.31641	1.334904	1.620416	366.17	212.94	746.44	826.53	135.26	298.76	0.955798	0.9712933	987.9654
11	0.985982	94.27	10.45863	1.362819	1.649852	368.17	215.93	755.92	838.27	138.09	305.66	0.972395	0.9851455	1003.964
12	0.997933	95.21	10.48187	1.369038	1.656147	368.56	216.45	757.75	840.61	138.72	307.13	0.976031	0.9884115	1007.121
13	1.063606	100.34	10.59992	1.406139	1.690101	370.71	219.20	766.62	851.83	142.48	315.14	0.996869	1.0080329	1022.094
14	1.065694	100.48	10.60556	1.40724	1.691032	370.78	219.31	766.96	852.27	142.59	315.35	0.997475	1.0092712	1022.668
15	1.086815	101.92	10.66386	1.418313	1.700301	371.59	220.43	770.54	856.85	143.71	317.45	1.003578	1.0145315	1028.602
16	1.092509	102.29	10.68043	1.421168	1.702761	371.80	220.67	771.53	858.19	144.00	317.99	1.005149	1.0159404	1030.323

Table 14 – Off-design simulation results

The deviation in the values can be attributed to the following features of the model. First, the bleed mass flow from the compressor for turbine cooling is assumed to be unchanged at high and low operating speeds, which is not correct. Also, the compressor bleed-off, which is used to avoid surging of the compressors during low air mass flows, is not included in the model. And this offsets the compressor and turbine operating point to an incorrect value, resulting in the gas path values and spool speeds to vary as well. Unfortunately, in the absence of detailed bleed schedule, this issue is difficult to solve.

Secondly, the lack of interstage bleed and cooling of the turbomachinery and the liner cooling of the combustion chamber are not included in the present TRANSEO modules. This affects the temperatures and pressures at the exit of these components, thereby creating the variations from the test report. Finally, during the low fuel flow conditions, the LP compressor experienced surge phenomenon, which shows the capability of the dynamic modelling methodology in TRANSEO. But this also demonstrated the need for bleed-off schedule for the compressors, without which, the results at low flow conditions could vary significantly.

SUMMARY AND DISCUSSIONS

The research activities conducted till date has resulted in the following results.

1) Development of a multi-stage axial compressor model capable of simulating surge and interstage bleed.
2) Development of a high-bypass turbofan model using the in-house dynamic simulation tool, TRANSEO.

The models have been validated against experimental data available in public domain and are found to be satisfactory. Further improvements to the models in order to develop the dynamic models of propulsion systems that utilize Pressure Gain Combustion technology, along with the necessary control concepts, is the ongoing activity of the project. This includes, but not limited to:

a) Incorporation into TRANSEO the multistage turbomachinery models with interstage bleed and cooling.
b) Development of reduced order model of Pressure Gain Combustors for TRANSEO.
c) Improved bleed and blade cooling control, including blade clearance control.
d) Engine start-up, shutdown and re-ignition sequence modelling using TRANSEO.

The research activities mentioned in this report demonstrate the capabilities of TRANSEO code to simulate gas turbine engines for propulsion activities. With the necessary improvements, modelling propulsion systems with pressure gain combustion is clearly within the domain of this simulation tool.

REFERENCES

[1] Kirner, R., Raffaelli, L., Rolt, A., Laskaridis, P., Doulgeris, G., and Singh, R., 2015, "An Assessment of Distributed Propulsion: Advanced Propulsion System Architectures for Conventional Aircraft Configurations," Aerosp Sci Technol, **46**, pp. 42–50.

[2] Corporan, E., Edwards, T., Stouffer, S., Hendershott, T., DeWitt, M., Klingshirn, C., West, Z., Bruening, C., and Striebich, R., 2017, "Impacts of Fuel Properties on Combustor Performance, Operability, and Emissions Characteristics," *AIAA SciTech Forum - 55th AIAA Aerospace Sciences Meeting*.

[3] Ranasinghe, K., Guan, K., Gardi, A., and Sabatini, R., 2019, "Review of Advanced Low-Emission Technologies for Sustainable Aviation," Energy, **188**, p. 115945.

[4] Jafari, S., and Nikolaidis, T., 2018, "Thermal Management Systems for Civil Aircraft Engines: Review, Challenges and Exploring the Future," Applied Sciences (Switzerland), **8**(11).

[5] Grönstedt, T., Xisto, C., Sethi, V., Rolt, A., Rosa, N. G., Seitz, A., Yakinthos, K., Donnerhack, S., Newton, P., Tantot, N., Schmitz, O., and Lundbladh, A., 2016, "Ultra Low Emission Technology Innovations for Mid-Century Aircraft Turbine Engines," *Proceedings of the ASME Turbo Expo*.

[6] Pollock, T. M., 2016, "Alloy Design for Aircraft Engines," Nat Mater, **15**(8).

[7] Heiser, W. H., and Pratt, D. T., 2002, "Thermodynamic Cycle Analysis of Pulse Detonation Engines," J Propuls Power, **18**(1), pp. 68–76.

[8] Neumann, N., and Peitsch, D., 2019, "Potentials for Pressure Gain Combustion in Advanced Gas Turbine Cycles," Applied Sciences (Switzerland), **9**(16).

[9] Braun, E. M., Lu, F. K., Wilson, D. R., and Camberos, J. A., 2013, "Airbreathing Rotating Detonation Wave Engine Cycle Analysis," Aerosp Sci Technol, **27**(1), pp. 201–208.

[10] Stathopoulos, P., 2018, "Comprehensive Thermodynamic Analysis of the Humphrey Cycle for Gas Turbines with Pressure Gain Combustion," Energies (Basel), **11**(12).

[11] Davis Jr, M. W., 1987, *A Stage-by-Stage Post-Stall Compression System Modeling Technique: Methodology, Validation, and Application*, Virginia Polytechnic Institute and State University.

[12] Moore, F. K., and Greitzer, E. M., 1986, "A Theory of Post-Stall Transients in Axial Compression Systems: Part 1—Development of Equations," J Eng Gas Turbine Power, **108**(1).

[13] Greitzer, E. M., and Moore, F. K., 1986, "A Theory of Post-Stall Transients in Axial Compression Systems: Part II—Application," J Eng Gas Turbine Power, **108**(2).

[14] Gamache, R. N., 1985, *Axial Compressor Reversed Flow Performance.*, AIR FORCE INST OF TECH WRIGHT-PATTERSON AFB OH.

[15] Haynes, J. M., Hendricks, G. J., and Epstein, A. H., 1994, "Active Stabilization of Rotating Stall in a Three-Stage Axial Compressor," J Turbomach, **116**(2).

[16] Cravero, C., and Massardo, A., 2001, *A Gas Turbine Compressor Simulation Model for Inclusion of Active Control Strategies*, GENOVA UNIV (ITALY).

[17] Massardo, A. F., Giusto, C., and Ghiglino, F., 1997, "Stage Performance Influence on Dynamic Simulation of Gas Turbine Compressors," Aircraft Engineering and Aerospace Technology, **69**(6).

[18] Soria, C., 2014, "Gas Turbine Shaft Over-Speed/Failure Modelling: Aero/Thermodynamics Modelling and Overall Engine System Response."

[19] Traverso, A., 2005, "TRANSEO Code for the Dynamic Performance Simulation of Micro Gas Turbine Cycles," *Proceedings of the ASME Turbo Expo*.

[20] Traverso, A., Massardo, A. F., and Scarpellini, R., 2006, "Externally Fired Micro-Gas Turbine: Modelling and Experimental Performance," Appl Therm Eng, **26**(16).

[21] Ferrari, M. L., Liese, E., Tucker, D., Lawson, L., Traverso, A., and Massardo, A. F., 2007, "Transient Modeling of the NETL Hybrid Fuel Cell/Gas Turbine Facility and Experimental Validation," J Eng Gas Turbine Power, **129**(4).

[22] Lambruschini, F., Liese, E., Zitney, S. E., and Traverso, A., 2016, "Dynamic Model of a 10 Mw Supercritical CO2 Recompression Brayton Cycle," *Proceedings of the ASME Turbo Expo*.

[23] Traverso, A., 2004, *TRANSEO: A New Simulation Tool for Transient Analysis of Innovative Energy Systems: Ph. d. Thesis*.

[24] Alexiou, A., and Mathioudakis, K., 2006, "Gas Turbine Engine Performance Model Applications Using an Object-Oriented Simulation Tool," *Turbo Expo: Power for Land, Sea, and Air*, pp. 109–116.

[25] Khalil, E. E., El-Sayed, A. F., and Abdelghany, E. S., 2013, "Effect of Bleed Air on Performance of Turbofan Engines," *51st AIAA Aerospace Sciences Meeting Including the New Horizons Forum and Aerospace Exposition 2013*.

[26] Sankar, B., Subramanian, T., Shah, B., Vanam, V., Jana, S., Ramamurthy, S., Satpathy, R., Sahoo, B., and Yadav, S., 2013, "Aero-Thermodynamic Modelling and Gas Path Simulation for a Twin Spool Turbo Jet Engine," *ASME 2013 Gas Turbine India Conference, GTINDIA 2013*.

[27] Carcasci, C., Piola, S., Canepa, R., and Silingardi, A., 2015, "Gas Turbine Integrated Conceptual Design Approach," *Proceedings of the ASME Turbo Expo*.

[28] Carcasci, C., Facchini, B., Gori, S., Bozzi, L., and Traverso, S., 2006, "Heavy Duty Gas Turbine Simulation: Global Performances Estimation and Secondary Air System Modifications," Turbo Expo: Power for Land, Sea, and Air, **42398**, pp. 527–536.

[29] Martins, D. A. R., 2015, "Off-Design Performance Prediction of the Cfm56-3 Aircraft Engine," Tecnico Lisboa MSc Thesis.

[30] Ridaura, J. A. R., 2014, "Correlation Analysis between HPC Blade Chord and Compressor Efficiency for the CFM56-3," Portugal: sn.

[31] European Aviation Safety Agency, 2008, *EASA-Certificate Sheet (E.066)*.

[32] Kurzke, J., 2005, "How to Create a Performance Model of a Gas Turbine from a Limited Amount of Information," *Proceedings of the ASME Turbo Expo*.

[33] Oates, G. C., 1997, “SAE Gas Turbine Engine Notation,” *Aerothermodynamics of Gas Turbine and Rocket Propulsion*.

[34] Philpot, M. G., 1992, *Practical Considerations in Designing the Engine Cycle*, ROYAL AEROSPACE ESTABLISHMENT FARNBOROUGH (UNITED KINGDOM), Farnborough (United Kingdom).

[35] Saravanamuttoo, H. I. H., Rogers, G. F. C., and Cohen, H., 2001, “Gas Turbine Theory (5th Ed.),” Gas Turbine Theory (5th Ed.).

APPENDIX 1

	Property	Mass flow	Temperature	Pressure
Station	Station Details	% variation	% variation	% variation
0	Ambient		0.00	0.00
2	Fan intake	0.26	0.00	0.00
13	Fan outlet	0.00	-0.04	-0.09
21	core inlet	1.61	0.00	0.00
22	LPC inlet	1.61	0.00	0.00
24	LPC outlet	1.61	-0.25	-1.11
25	HPC inlet	1.61	-0.25	0.91
3	HPC outlet	3.69	-1.50	-3.55
31	CC inlet	1.62	-1.50	1.67
4	CC outlet	1.57	-1.40	1.52
41	HPT inlet	6.92	-5.26	1.52
44	HPT outlet	1.59	-3.76	-2.89
45	LPT inlet	1.57	-3.78	-1.91
5	LPT outlet	1.57	-1.72	-3.96
8	Core nozzle throat	1.57	-1.72	-2.99
18	Bypass nozzle throat	0.00	-0.03	2.47

Table 15 - Variation of thermodynamic properties for Type-1 model

	Property	Mass flow	Temperature	Pressure
Station	Station Details	% variation	% variation	% variation
0	Ambient		0.00	0.00
2	Fan intake	-0.04	0.00	0.00
13	Fan outlet	0.01	-0.03	-0.09
21	core inlet	-0.28	0.00	0.00
22	LPC inlet	-0.28	0.00	0.00
24	LPC outlet	-0.28	-0.27	-1.20
25	HPC inlet	-0.28	-0.27	0.82
3	HPC outlet	1.75	-2.17	-5.93
31	CC inlet	1.70	-2.17	-0.62
4	CC outlet	1.66	-1.71	-0.98
41	HPT inlet	1.66	-2.65	-0.98
44	HPT outlet	-3.41	-0.55	-2.04
45	LPT inlet	1.67	-2.99	-1.05
5	LPT outlet	1.67	-1.02	-3.70
8	Core nozzle throat	1.67	-1.02	-2.73
18	Bypass nozzle throat	0.01	-0.03	2.47

Table 16 - Variation of thermodynamic properties for Type-2 model

APPENDIX 2

1) Calculate nozzle pressure ratio, NPR

$$\mathbf{NPR} = \frac{\mathbf{P\_total\_in}}{\mathbf{P_0}} \tag{4.2}$$

2) Calculate nozzle critical pressure ratio, NPR$_{cr}$

$$\mathbf{NPR_{cr}} = \frac{\mathbf{P\_total\_in}}{\boldsymbol{P_c}} = \frac{\mathbf{1}}{\left[\mathbf{1} - \frac{\mathbf{1}}{\boldsymbol{\eta_j}}\left(\frac{\boldsymbol{\gamma} - \mathbf{1}}{\boldsymbol{\gamma} + \mathbf{1}}\right)\right]^{\left(\frac{\boldsymbol{\gamma}}{\boldsymbol{\gamma}-\mathbf{1}}\right)}} \tag{4.3}$$

3) If **NPR** $< \mathbf{NPR_{cr}}$, then the nozzle is not choked. Use equations (4.4), (4.5) & (4.6) to find the nozzle thrust.

$$\mathbf{\Delta T = T\_total\_in - T\_static\_in} = \boldsymbol{\eta_j}\mathbf{T\_total\_in}\left[\mathbf{1} - \left(\frac{\mathbf{1}}{\mathbf{NPR}}\right)^{\frac{\boldsymbol{\gamma}-\mathbf{1}}{\boldsymbol{\gamma}}}\right] \tag{4.4}$$

$$\mathbf{V\_exit} = \sqrt{\mathbf{2C_p\Delta T}} \tag{4.5}$$

$$\textbf{Nozzle Thrust = Nozzle mass flow rate x (V\_exit - V\_flight)} \tag{4.6}$$

4) If **NPR** $\geq \mathbf{NPR_{cr}}$ **,** then the nozzle is choked. Use equations (4.7), (4.8), (4.5), (4.10) & (4.10) to find the nozzle thrust.

$$\mathbf{T\_static\_in} = \left(\frac{\mathbf{2}}{\boldsymbol{\gamma} + \mathbf{1}}\right)\mathbf{T\_total\_in} \tag{4.7}$$

$$\mathbf{\Delta T = T\_total\_in - T\_static\_in} \tag{4.8}$$

$$\mathbf{V\_exit} = \sqrt{\mathbf{2C_p\Delta T}} \tag{4.5}$$

$$\boldsymbol{P_c} = \frac{\mathbf{P\_total\_in}}{\mathbf{NPR_{cr}}} \tag{4.9}$$

$$\textbf{Nozzle Thrust} = (\boldsymbol{Nozzle\ mass\ flow\ rate\ x}(\mathbf{V\_exit\text{-}V\_flight})) + (\boldsymbol{Nozzle\ Throat\ Area\ x}\ (\boldsymbol{P_c} - \boldsymbol{P_0})) \tag{4.10}$$

5) Net thrust is the sum of the nozzle thrusts from core engine nozzle and bypass nozzle.
6) TSFC is calculated using equation (4.11).

$$\mathbf{TSFC} = \frac{\textbf{Mass flow rate of fuel}}{\textbf{Net Thrust}} \tag{4.11}$$

The unknown parameter, nozzle efficiency ($\boldsymbol{\eta_j}$), is obtained from the engine performance reported in literature.